N O T I C E

THIS DOCUMENT HAS BEEN REPRODUCED FROM MICROFICHE. ALTHOUGH IT IS RECOGNIZED THAT CERTAIN PORTIONS ARE ILLEGIBLE, IT IS BEING RELEASED IN THE INTEREST OF MAKING AVAILABLE AS MUCH INFORMATION AS POSSIBLE

DEPARTMENT REPORT UWME-DR-901-103-1

ENERGY ABSORPTION MECHANISMS DURING CRACK PROPAGATION in METAL MATRIX COMPOSITES

Daniel P. Murphy
Donald F. Adams

October 1979

(NASA-CR-162574) ENERGY ABSORPTION MECHANISMS DURING CRACK PROPAGATION IN METAL MATRIX COMPOSITES Interim Report, Aug. 1978 - Aug. 1979 (Wyoming Univ.) 92 p HC A05/MF A01 CSCL 11F G3/26

N80-15232

Unclas 45140

TECHNICAL REPORT

NASA-Lewis Research Center

Grant No. NSG-3217

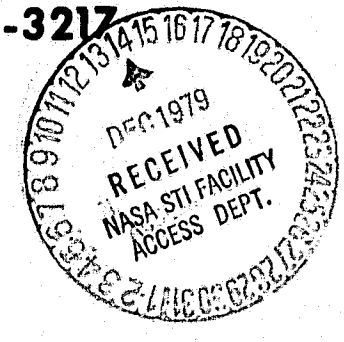

Approved for Public Release; Distribution Unlimited

COMPOSITE MATERIALS RESEARCH GROUP
DEPARTMENT of MECHANICAL ENGINEERING
University of Wyoming Laramie, Wyoming 82071

DEPARTMENT REPORT
UWME-DR-901-103-1

ENERGY ABSORPTION MECHANISMS DURING CRACK PROPAGATION IN METAL MATRIX COMPOSITES

ANNUAL TECHNICAL REPORT
NASA - LEWIS RESEARCH CENTER
GRANT NO. NSG-3217

OCTOBER 1979

DANIEL P. MURPHY
DONALD F. ADAMS

COMPOSITE MATERIALS RESEARCH GROUP
MECHANICAL ENGINEERING DEPARTMENT
UNIVERSITY OF WYOMING
LARAMIE, WYOMING 82071

APPROVED FOR PUBLIC RELEASE; DISTRIBUTION UNLIMITED

PREFACE

This Annual Technical Report presents research performed during the first year of NASA-Lewis Grant NSG-3217, which was initiated on August 1, 1978. The grant is continuing, presently being budgeted for the second year. The NASA-Lewis Technical Monitor since the inception of this grant has been Dr. J. A. DiCarlo of the Materials Science Branch.

The study is being performed within the Composite Materials Research Group at the University of Wyoming. Principal Investigators are Mr. Daniel P. Murphy, Graduate Student, and Dr. Donald F. Adams, Professor, both of the Mechanical Engineering Department. Mohamed M. Monib and Brent G. Schaffer, Graduate Students in Mechanical Engineering, have also made significant contributions.

CONTENTS

Section		Page
1.	INTRODUCTION	1
2.	SUMMARY	5
3.	ANALYSIS	8
	3.1 THE FINITE ELEMENT METHOD AS AN ANALYSIS	8
	3.2 FINITE ELEMENT MICROMECHANICS ANALYSIS	10
	3.3 CRACK INITIATION AND PROPAGATION	12
	3.4 DEVELOPMENT OF THE BROKEN FIBER, LONGITUDINAL SECTION MODEL	25
	3.5 DEVELOPMENT OF THE TRANSVERSE SECTION MODEL	31
4.	MATERIAL PROPERTIES	33
5.	NUMERICAL RESULTS	35
	5.1 AXIAL LOADING OF THE 45° SECTION LONGITUDINAL MODEL	36
	5.2 AXIAL LOADING OF THE 90° SECTION LONGITUDINAL MODEL	45
	5.3 AXIAL LOADING OF THE TRANSVERSE SECTION MODEL	53
6.	FUTURE WORK	64
	REFERENCES	66
	APPENDIX A. FINITE ELEMENT FORMULATION OF THE MICRO-MECHANICS ANALYSIS COMPUTER PROGRAM	69

SECTION 1

INTRODUCTION

It is widely recognized that crack initiation and propagation in fiber-reinforced composite materials is necessarily quite different from that in homogenous solids, and that most applications of classical linearly elastic fracture mechanics have not been satisfactory.

The inhomogenous nature of fiber-reinforced materials strongly suggests the use of so-called micromechanical analysis techniques, wherein the interactions of the individual reinforcing fibers with the surrounding matrix material are considered. Specifically, if sufficient insight into the geometrical effects can be gained, the energy absorption due to crack initiation and growth in a unidirectional boron/aluminum composite can be characterized with a two-dimensional micromechanics analysis. This is the primary objective of the present study.

The first-year effort reported here has been directed at investigating the response of a unidirectional boron/aluminum composite containing a fiber flaw site or discontinuity. Tensile loading in the direction of the fiber axes is of primary interest, although transverse loading has also been analyzed. To approximate the behavior of a metal matrix composite under these conditions, two features are of major importance to a micromechanics analysis:

- The ability to model the full elastic-plastic range of the matrix material and modify it to account for changes in temperature.
- The availability of a procedure for approximating crack

growth in the matrix material.

The finite element micromechanics program previously developed at the University of Wyoming [1] possessed the first of these features at the time that the present grant was awarded, and a crack propagation capability was incorporated during the fourth quarter of this first-year effort.

A survey of the literature available on the topics of micromechanics analyses and the effect of flaws in unidirectional metal matrix composites has yielded some valuable information, and has provided insight into the problems involved. But the exact problem dealt with in this grant study does not appear to have been attempted before.

Among previous analysis efforts is a series of two reports published in 1973 by Adams [2], and Repnau and Adams [3], in which a finite element micromechanics program was developed, incorporating both elastoplastic capability and crack propagation. A unidirectional boron/aluminum composite was studied, although no flaw sites were incorporated and the model grid represented a section of the composite which was transverse to the fiber axes. Also, because a plane strain solution was assumed, only transverse loading could be studied. Material modifications to reflect environmental changes were also not available in these programs.

Another effort was that of Ko [4] in 1977. His analysis was of an axially loaded boron/aluminum composite using the NASTRAN finite element analysis program as a micromechanics tool. His model consisted of a single boron fiber surrounded by an annular section of aluminum matrix. Axisymmetric finite elements were employed and discontinuitites in both the fiber and the matrix were studied. However, the NASTRAN solution did not incorporate elastoplastic material response, nor was any sort of crack propagation scheme used.

Akbarzadeh [5] undertook a micromechanics analysis of flawed unidirectional composites in 1978. The material he studied was E-glass/epoxy and the flaws were taken to be discontinuous fibers. Again, the NASTRAN finite element program was employed, and no elastoplastic deformation or crack growth was considered. His finite element grid represented a cross-sectional cut transverse to the fiber axes and all loading was confined to the plane of that section, i.e., there was no axial loading. Akbarzadeh's finite element grid was very fine, and his analysis yielded valuable information concerning the elastic microstress state in composites with different fiber packing geometries and densities, and the effects of varying the elastic moduli of the constituent materials.

Finally, there has been a limited amount of experimental work done in the area of interest dealt with in this report. One of the more important of these was by Awerbuch and Hahn [6], in which the crack tip damage and fracture toughness of axially loaded unidirectional boron/aluminum composites was studied. Awerbuch and Hahn prepared tension coupons of boron/aluminum in which a center notch was machined, cutting several fibers and the aluminum matrix between them. Among the data generated by their efforts are some describing the deformation of the aluminum matrix surrounding the last cut fiber at the edge of the notch. This has been of some help in evaluating the results of the present analysis.

The present study has yielded valuable information about the analytical approach to the problem of energy absorption in a flawed metal matrix composite. The analysis is a quasi-three-dimensional formulation (see Section 3), which allows traction loads to be applied to threee mutually perpendicular surfaces ot a two-dimensional finite element array. This program in its present form can predict the microstress state of a metal

matrix composite with flaws quite well, and provides information regarding the energy absorption resulting from plastic deformation and crack growth at such flaw sites. However, the full characterization of this problem involves the rather complex geometry resulting from an array of cylindrical fibers inbedded in an elastoplastic matrix, and the final solution would appear to require a three-dimensional analysis. The follow-on second-year study will consider such an analysis, incorporating all of the features of the present analysis into a three-dimensional formulation.

SECTION 2

SUMMARY

Considerable progress in the investigation of the energy absorption and the microstress state of unidirectional metal matrix composites has been made to date. Further development of the analytical procedures described in this report, together with a carefully conceived and executed experimental program is expected to lead to a reliable means of predicting the strength and toughness of these composite materials under actual conditions of manufacture and service. That is, given certain statistical parameters which define the quality of the constituents, a prediction of the energy capacity of the composite could be made.

As was discussed in Section 1, and confirmed by an on-going literature survey, the particular problem being dealt with here, and the analytical procedures employed, make this study unique. A finite element analysis program is used to determine the stress-strain state of a unidirectional, metal matrix composite material. A rather comprehensive description of the theoretical foundations and the special capabilities of this computer program is provided in Appendix A. This program has been modified, and is in the process of being expanded to make it more suitable for the study of energy absorption mechanisms in axially loaded metal matrix composite materials containing flaws in the form of microcracks in the matrix material, or discontinuities in the fibers. The two most important energy absorption mechanisms being studied are plastic deformation due to the stress concentrations arising out of a material flaw, and growth of any cracks initiated by such a flaw.

A major problem in investigating the microstress state of unidirectional composites is related to their geometrical inhomogeneity, i.e., the fact that a detailed representation of the stress state in and around the filaments embedded in an inelastic matrix is required. While the finite element analysis program employed is quasi-three-dimensional in that it can be loaded in all three coordinate directions and the resulting stresses and strains computed, the actual modeling of the region of interest is essentially a two-dimensional representation. As described in Sections 3.3 and 3.4, an attempt to account for the complex geometry of the problem was made by constructing two types of finite element arrays. One is the "longitudinal" model, which represents a cross-sectional cut through the composite running parallel to the axes of the boron fibers. This model is particularly useful in studying the effects of discontinuous fibers, or fibers with regions of reduced strength. In addition, the presence of cracks or voids in the metal matrix can be modeled and their effect on the axial strength, and to some extent the transverse strength, of the material can be studied.

The other type of model developed will be referred to the "transverse" section model, and depicts a cross-sectional cut perpendicular to the fiber axes of the composite. This model is well-suited for studying the effects of transverse loading of the composite material, and the influence of the circular cross section of the fibers is fully accounted for. Fiber flaws and matrix flaws can be completely characterized for transverse loading. Due to the generalized plane strain formulation used in the analysis, it is possible to load the transverse model in the axial, or z-directions. Unfortunately, with this mode of loading, it has not been possible to study to stress concentrating effects of flaws and discon-

tinuities. This is due to the fact that all element displacements out of the plane of the model must be equal (see Section A.2 of the Appendix), and variations in axial stress are thus due to Poisson effects and differences in material properties only.

The longitudinal models have been useful in studying the effects of flaws on the axial strength of unidirectional composites, as detailed in Sections 5.1 and 5.2. The extent of plastic deformation around a flaw and the effects on the load redistribution among the surrounding fibers can be characterized quite well. For this model too, considerations have to be made regarding the geometry of the composite. As discussed in Section 3.3, this leads to the two configurations of the longitudinal model which are necessary to characterize a square or rectangluar fiber array.

Crack initiation and propagation are clearly important considerations in the study of energy absorption in flawed materials. This capability has been added to the micromechanics analysis, and is described in Section 3.2. Unfortunately, a numerical inconsistency was discovered near the end of this first-year program, and subsequent corrections to the program have not yet been fully debugged. Consequently, numerical results of crack propagation in a unidirectional, metal matrix composite will be presented in the next quarterly report.

SECTION 3

ANALYSIS METHOD

3.1 THE FINITE ELEMENT METHOD AS A MICROMECHANICS TOOL

The scope of the following analysis is to determine the internal stress distribution in a unidirectional fiber-reinforced, metal matrix composite material subjected to mechanical loadings and variations in temperature. In addition, the effects of material flaws or discontinuities and their subsequent propagation through the material continuum are to be characterized.

The typical unidirectional composite has a nonhomogenous internal structure that consists of at least two distinct phases, i.e., a homogenous matrix material reinforced by isotropic or transversely isotropic fibers. Transverse isotropy refers to the condition in which the axial properties of the fiber (e.g., strength and modulus) differ significantly from those in a plane normal to the fiber axis. In most unidirectional composites, boron/aluminum included, the reinforcing fibers are much stronger and possess a much higher axial elastic modulus than the surrounding matrix. The nonhomogenous nature of such a composite, together with the geometrical considerations of a cylindrical filament embedded in a matrix and containing a microscopic flaw, results in a boundary value problem of such compexity that a classical closed form continuum solution to evaluate the microstress state would be impractical. As a result, investigators for the last 12 to 14 years have formulated numerical schemes to evaluate microstresses in unidirectional composites. In one of the earlier efforts, Adams and Doner [7] applied finite difference techniques

to their micromechanical studies. More recently, the finite element method has emerged as the most versatile tool available for such studies, as demonstrated by numerous investigators [8-18].

The finite element analysis method is based on the concept of discretizing a material continuum into an assembly of "elements" of "finite" size. The individual elements are assembled into a network representing the continuum by joining them at predetermined points or "nodes" along their boundaries. For any element, approximate functions representing either stress, strain or the displacement field within that element can then be written. By a suitable choice of coefficients for these assumed field equations, a minimization of the potential energy of the system is achieved. To date, the assumed displacement field technique has been the most successful and the most generally applied [19]. For an assumed displacement field for the interior of an assembly of elements, minimization of the potential energy results in a set of simultaneous algebraic equations relating loads to displacements. These equations can readily be solved with modern digital computers. This procedure is explained in rigorous detail by Heubner [19] and Zienkiewicz [20] wherein they point out that the finite element method is as useful in solving thermodynamics and fluid mechanics problems as it is in solid mechanics, the only difference being that functionals other than potential energy must be minimized.

One of the great advantages of this method is that the approximate field equations need only satisfy the constraints of the individual elements. An important consequence of this situation is that equilibrium and compatibility conditions between the assumed fields of the individual elements must be met in order to insure convergence to a correct solution. These conditions are also thoroughly discussed and developed in texts by

Heubner [19], Cook [21], and Zienkiewicz [20].

The finite element method may be applied to any general three-dimensional problem, the primary limitation being one of computer capacity. In an effort to analyze rather complex structural configurations in sufficient detail, most analyses, including all micromechanics analyses to date, are reduced to two-dimensional problems, i.e., plane stress, plane strain, or generalized plane strain formulations. The analysis method used in the present study is a two-dimensional form incorporating a condition of generalized plane strain, which permits a specific loading to be applied in the third direction. This concept is discussed in detail in Section A.2 of Appendix A.

3.2 FINITE ELEMENT MICROMECHANICS ANALYSIS

The primary analytical tool used in the present study has been the micromechanics finite element analysis program developed by A. K. Miller while completing his Ph.D. studies at the University of Wyoming, which is described in considerable detail in Reference [1]. This program was created to investigate the microstress state in unidirectional composite materials subjected to transverse mechanical loads, thermal gradients, and dilatational stresses due to moisture absorption by polymeric matrix materials. Among the special features of this program are its ability to model the elastic-plastic stress-strain response of the isotropic matrix material, and in concert with the determination of thermal and moisture dilatational stresses, the functional dependence of the matrix material properties on temperature and moisture content. In other words, the elastic or plastic properties of any matrix material finite element are automatically computed to reflect the state of stress and the environmental conditions of temp-

erature and humidity. The adjustment of material properties is incorporated with the incremental loading technique that is employed in this program. Once the initial temperature, moisture content, and/or elastic stress level for the continuum have been specified, additional loads, be they mechanical or environmental, are introduced in increments small enough to permit close approximation of the nonlinear matrix material properties by small linear segments. A more detailed description of this technique is presented in Section A.5 of Appendix A.

The bulk of the elastoplastic formulation in the present analysis program stems from previous work done by Adams [2, 3, 18]. The development of the hygrothermal loading and material properties dependence was the subject of Miller's Ph.D. research [1], and the addition of crack initiation and crack propagation capability, to be discussed in detail in the following section, was performed by the present writers. The basis for this program is the procedure set down by Zienkiewicz [20], and in fact, the primary organization and flow of the present computer program closely follows the suggestions of Appendix A of that text. This flow and organization has subsequently been rather severely altered to include crack propagation capability.

The finite element used in this study is a modified version of the familiar constant strain or simplex triangle. For this element, a linear displacement field within each element is assumed, to arrive at a functional representation of the potential energy of the system, as referred to in Section 3.1 and described in Section A.2 of Appendix A. The constant strain triangular element has some well-known limitations, but for the purposes of micromechanics analyses, it is an acceptable, economic, and powerful tool. The trade-offs involved in the choice of the constant strain

triangular element instead of one of the higher order finite elements is covered quite well by Miller in Chapter 3 of Reference [1]. A brief description of the formulation of the constant strain triangular element in its generalized plane strain form is presented in Sections A.1 through A.3 of Appendix A. The manner in which loads are introduced to the finite element model is described in Section A.4 of Appendix A. A discussion of the concepts and procedure used to analyze the isotropic matrix material in the plastic zone, and the temperature/moisture dependence of the matrix material properties, is presented in Section A.5 of Appendix A. In the following Section 3.3, the concepts and methodology used to simulate the initiation and propagation of cracks in the composite material are briefly outlined, and the analytical relations along with the required sequence of operations in the computer program to accomplish this are presented.

3.3 CRACK INITIATION AND PROPAGATION

The purpose of the present study was to investigate the effects of flaws in unidirectional boron/aluminum composites, with the eventual goal of predicting the strength of such composites given a certain statistical distribution of internal flaws. These defects manifest themselves in two forms: a discontinuity in one or more boron fibers, or a localized void in the aluminum matrix. The loading condition of primary interest is that of tension applied parallel to the fiber axes. With suitable modification, a so-called longitudinal model was analyzed with the micromechanics program in its original form [22]. This permitted modeling of the flaw, generally a fiber discontinuity, and an evaluation of the resulting localized stress concentration and the local plastic deformation it caused. The redistribution of the load to the broken fiber could also be characterized, but only up to the point at which a matrix element failed (crack

initiation). What was necessary for further study of the load capability of the flawed composite was a crack propagation scheme. This capability would also permit a characterization of the energy required to isolate the defect in a "zone" of plastically deformed matrix material, or alternatively, the total energy capacity of the system at the point of catastrophic failure.

The approach to crack inititation and propagation taken here is known as the "failed element" approximation as employed by Adams [2, 3]. When an element in an area of high stress exhausts its strain energy capacity, it fails. From this, we assume that a "crack" has formed and has the dimensions of the failed element. This approximation has two implications, the most important of which is that a finite amount of material is removed from the system, which in an actual material is not the case. The other is that the crack is not likely to close up on itself in subsequent loading because of its exaggerated width. These effects can be minimized to a practical degree by making the finite element grid very fine and uniform in the area of anticipated crack initiation.

It is not enough to simply delete an element from the finite element grid when it reaches its ultimate stress. The finite element method involves the maintenance of force equilibrium at every node point in the array, as discussed in Section A.3 of Appendix A. This equilibrium must be maintained when an element fails or unloads. Thus, to represent the unloading due to element failure, node point loads which are equal and opposite in sense to those equivalent to the state of stress within the element at its failure level must be applied at its node points. In addition, the failed element's material properties must be set to zero, so that the element makes no further contribution to the global stiffness

matrix, and all of its computed values of stress and strain are set to zero. This insures that the element is completely unloaded and that no stresses will be developed in it in subsequent load increments.

The "reaction loads" applied to the node points of a failing element are computed in the following manner. Given the state of stress within an element at the time of failure, i.e., σ_x, σ_y, τ_{xy}, the statically equivalent forces acting at the mid-sides of the element, as illustrated in Figure 3.1 can easily be computed: (See for example pp 40-43, Reference [19].)

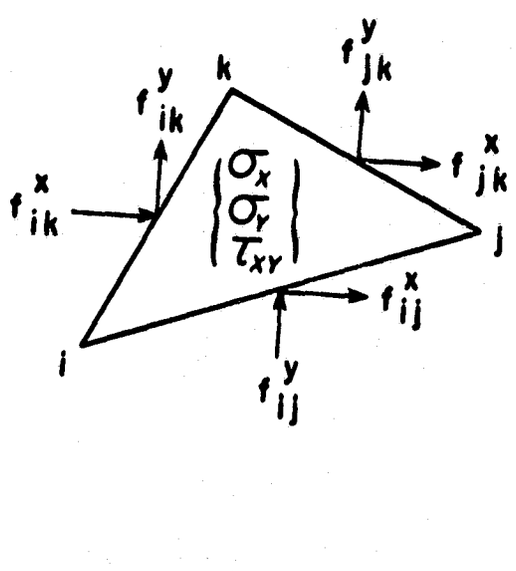

FIGURE 3.1
Force-Stress Relationships

$$
\begin{aligned}
f^x_{ij} &= \sigma_x y_{ji} + \tau_{xy} x_{ij} \\
f^y_{ij} &= \sigma_y x_{ij} + \tau_{xy} y_{ji} \\
f^x_{jk} &= \sigma_x y_{kj} + \tau_{xy} x_{jk} \\
f^y_{jk} &= \sigma_y x_{jk} + \tau_{xy} y_{kj} \\
f^x_{ik} &= \sigma_x y_{ik} + \tau_{xy} x_{ki} \\
f^y_{ik} &= \sigma_y x_{ki} + \tau_{xy} y_{ik}
\end{aligned}
\qquad (3\text{-}1)
$$

where the quantitites x_{ij}, y_{kj}, etc. are as defined in Figure 3.2, which identifies the important geometrical parameters of the generalized plane strain triangular element.

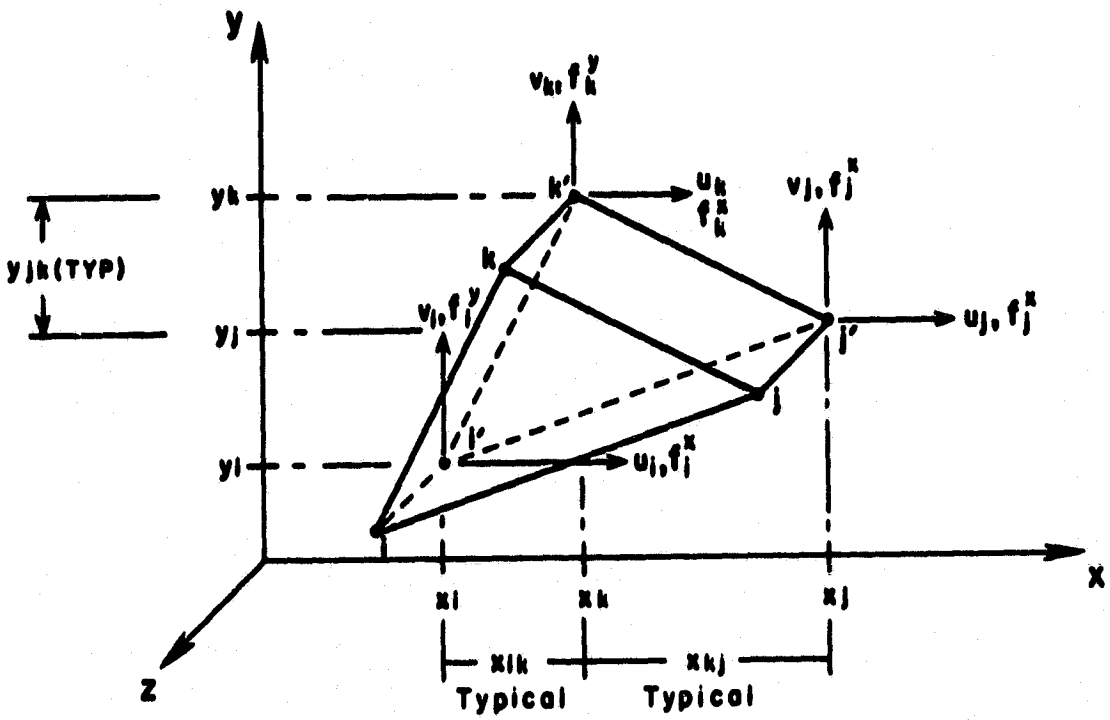

FIGURE 3.2

Typical Triangular Finite Element of Unit Thickness

These forces, when translated to the node points with their directions reversed, are the reaction loads required for the unloading of the element, and are shown below and illustrated in Figure 3.3.

$$
\begin{aligned}
R_i^x &= -\tfrac{1}{2}(f_{ij}^x + f_{ik}^x) \\
R_i^y &= -\tfrac{1}{2}(f_{ij}^y + f_{ik}^y) \\
R_j^x &= -\tfrac{1}{2}(f_{ij}^x + f_{jk}^x) \\
R_j^y &= -\tfrac{1}{2}(f_{ij}^y + f_{jk}^y) \\
R_k^x &= -\tfrac{1}{2}(f_{ik}^x + f_{jk}^x) \\
R_k^y &= -\tfrac{1}{2}(f_{ik}^y + f_{jk}^y)
\end{aligned}
\qquad (3\text{-}2)
$$

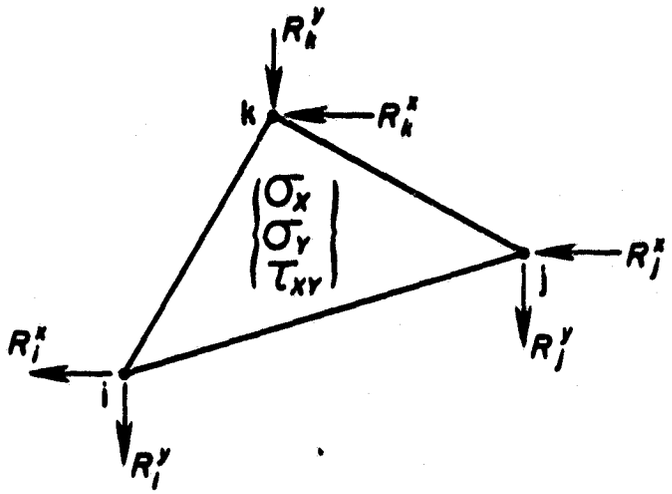

FIGURE 3.3

Node Point Reaction Loads Statically
Equivalent to Stresses in the Element

In the present analysis, element failure can occur in one of two modes: when both the computed octahedral shear stress and the plastic octahedral shear strain reach their maximum allowable values (maximum distortional energy criterion), or when the hydrostatic tensile stress in an element exceeds the tensile ultimate strength of the material. This second failure criterion is also known as failure due to ultimate cleavage, and failure occurs whenever a tensile principal stress exceeds the ultimate tensile strength.

Although loading increments are kept small once elements begin to enter the plastic region, it is unlikely that an element will fail exactly at the maximum value of an applied load increment. That is, the load increment will probably be more than sufficient to cause failure in the element. For this reason, it is desireable to scale down the load increment to the point of element failure. This fraction of the load increment required to cause an element to fail is referred to as the "Ratio" and its definition is clarified in Figure 3.4.

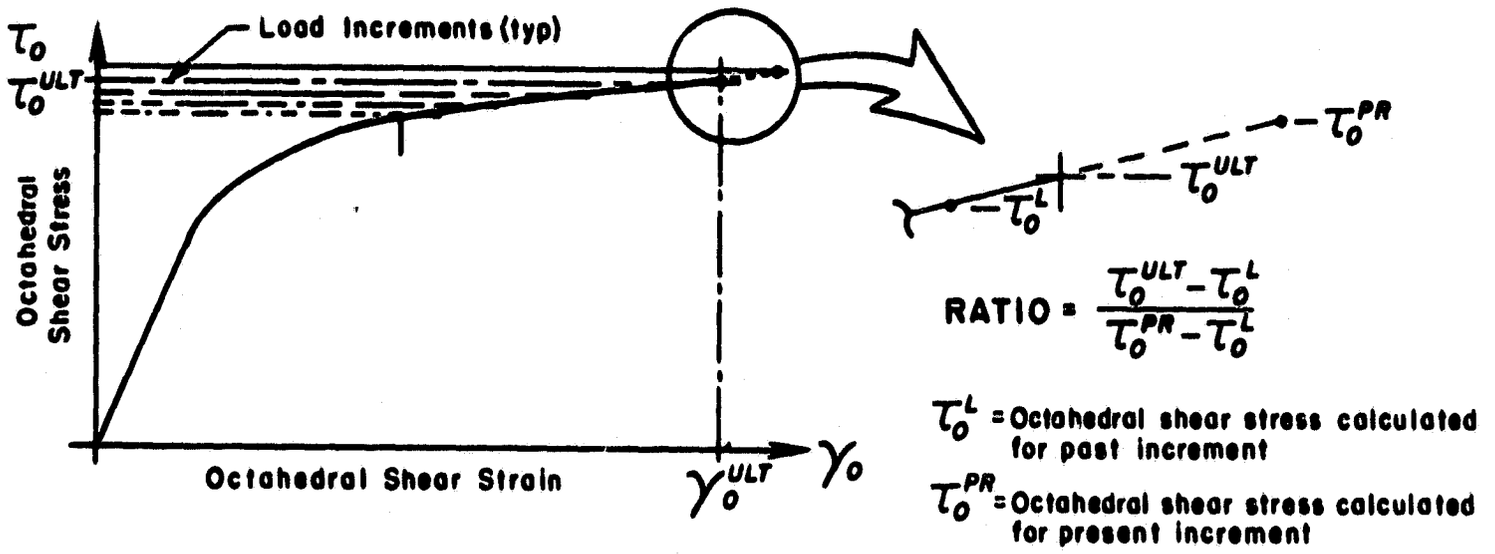

FIGURE 3.4

Determination of Increment Scale Factor (Ratio) for Element Failure

Once one or more elements have failed during a given loading increment, the crack propagation procedure is set into motion. This procedure will be outlined below and is illustrated in the flow chart shown in Figure 3.5.

The first operation to be performed in effecting crack growth is to identfy which element failure in a single load increment, if indeed more than one element has failed, required the greatest portion of that load increment to cause failure. The Ratio, as defined in Figure 3.4, is then computed for this element. This quantity is the fraction of the load increment that is necessary to fail all of the elements in that increment. It is now necessary to multiply all of the element stresses and nodal displacements that were computed as a result of the load increment application by this maximum value of Ratio. These reduced incremental quantities are then added to the sums of the stresses, displacements and strains in the normal manner

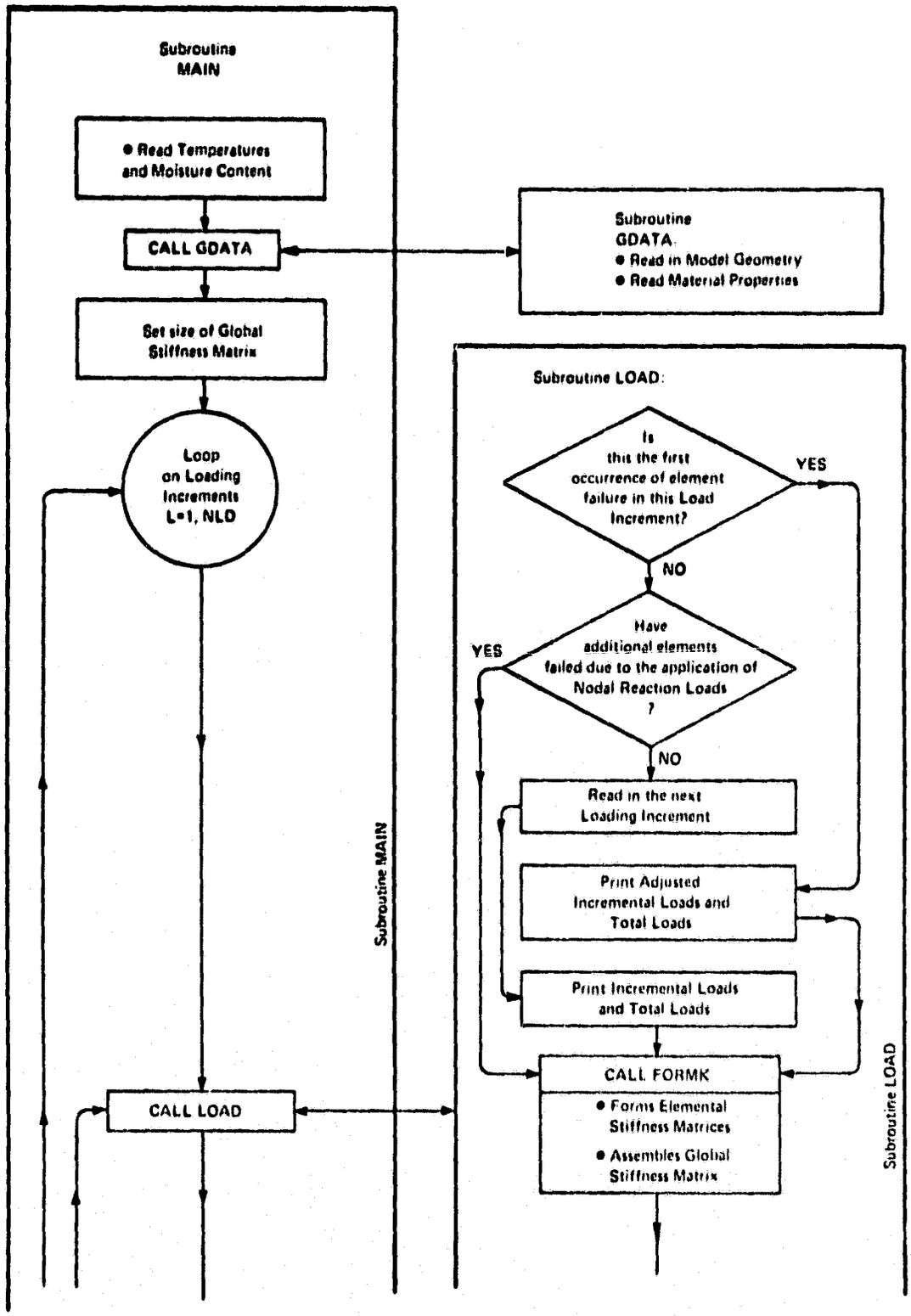

FIGURE 3.5

Flow Chart of the Micromechanics Analysis Computer Program, Crack Propagation Version

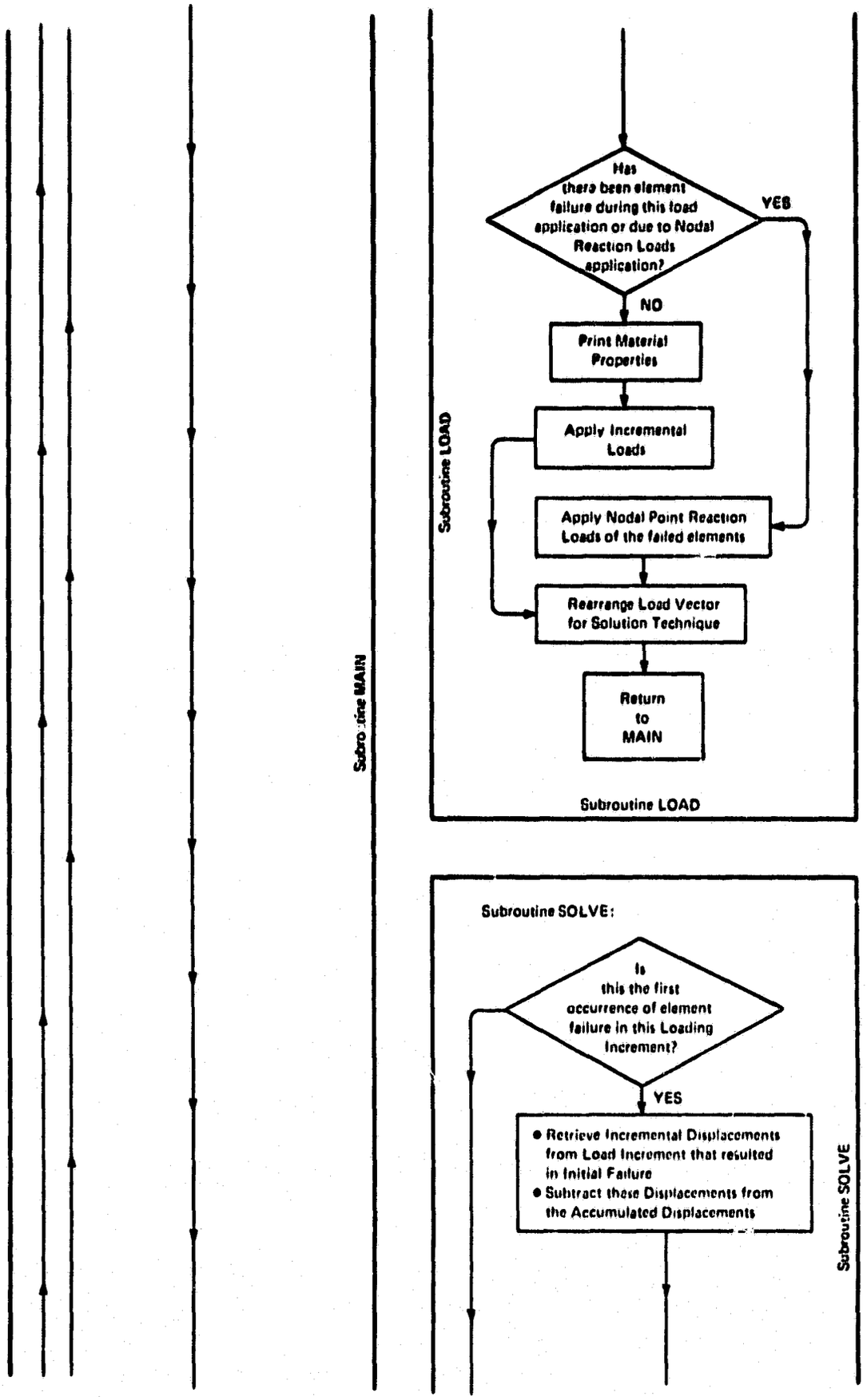

FIGURE 3.5 - Continued

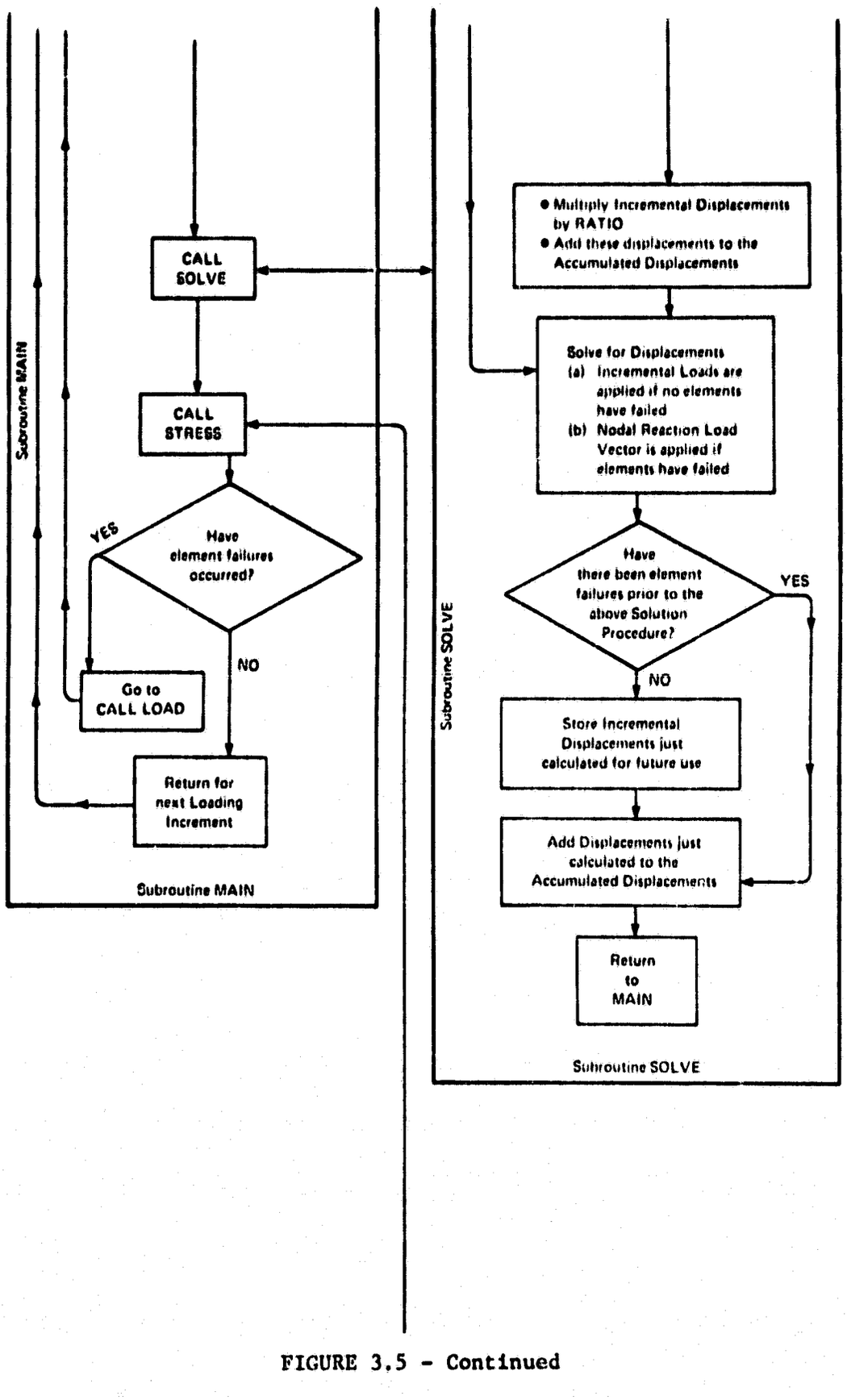

FIGURE 3.5 - Continued

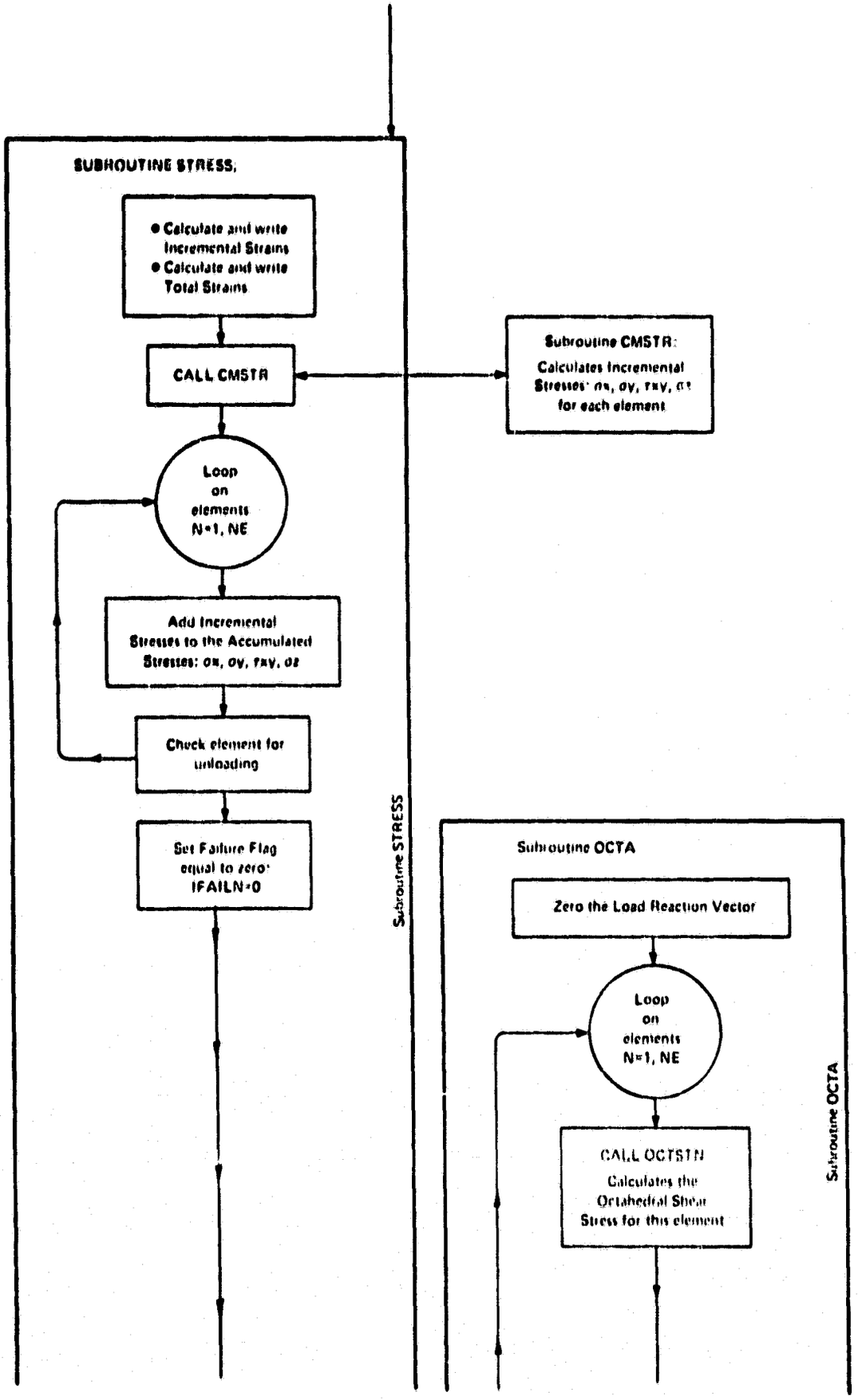

FIGURE 3.5 - Continued

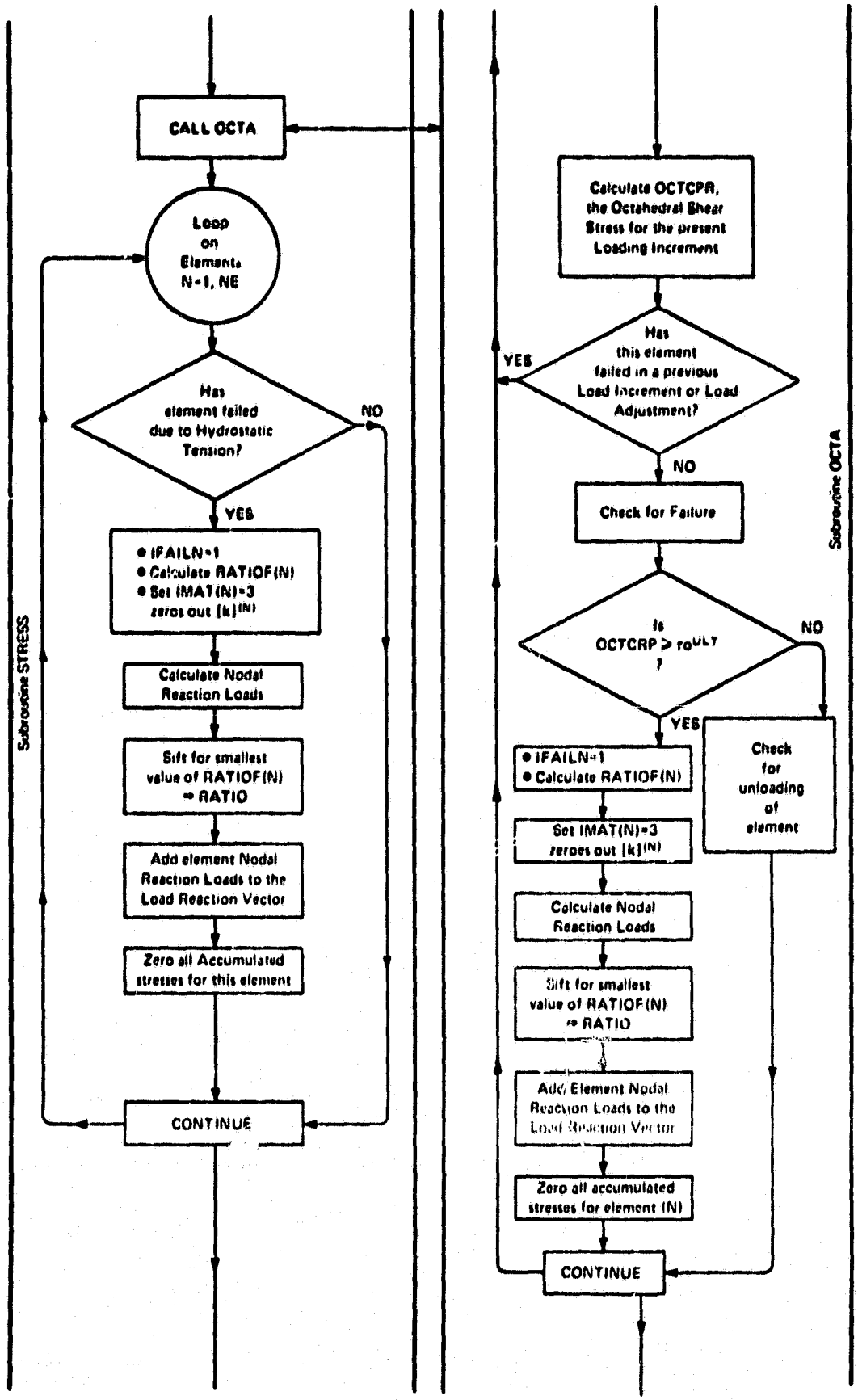

FIGURE 3.5 - Continued

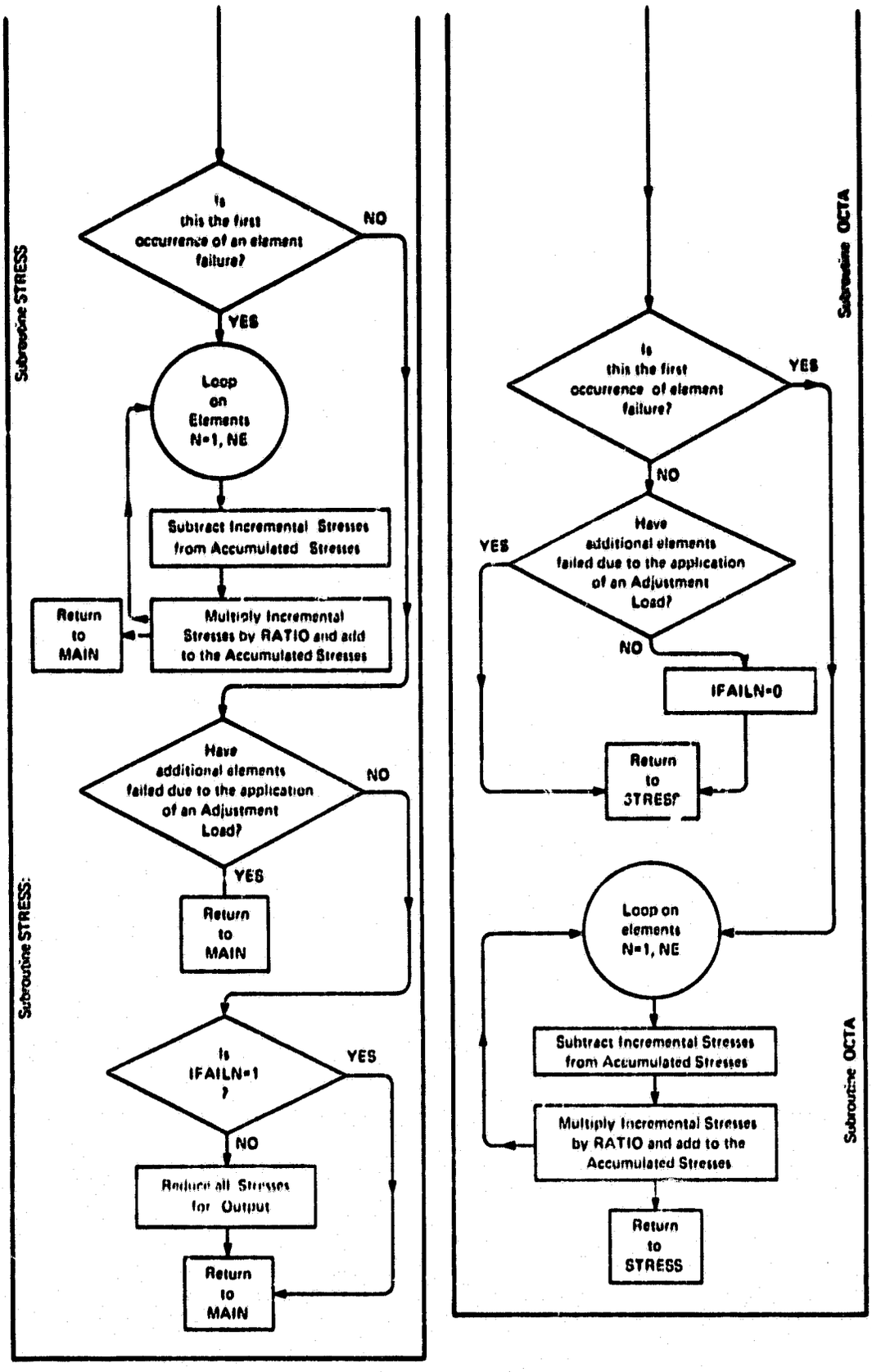

FIGURE 3.5 - Continued

to give "adjusted" quantities. The next step is to compute the nodal point reaction loads of the failed elements, using the adjusted accumulated stress values and the relationships of Equations 3-1 and 3-2. These forces become the "adjustment loads" which must be applied to the finite element model with the stiffnesses of the failed elements deleted from the global stiffness matrix (see Section A.3 of Appendix A). In this manner, the energy required to cause the element failure is redistributed into and absorbed by the remainder of the region being studied. This results in new increments of stress, strain and displacement being added to the accumulated values, but the operation is not counted as a load increment by the program. Of course, this adjustment loading may result in the failure of additional elements adjacent to those that have already failed, causing the crack to grow without the application of additional external loading. This is similar to the behavior of a crack that has reached its critical length. When this occurs, all the elements that have failed have nodal reaction loads computed from the stresses resulting from the adjustment load application, i.e., no ratioing takes place. These elements are then deleted from the global stiffness matrix and their nodal reaction loads are applied to the model consisting of the remaining elements. This procedure is repeated until no further element failures occur as the result of an adjustment load application, or until catastrophic failure of the finite element model occurs. Catastrophic failure is assumed to have occurred when a progression of failed and deleted elements results in the division of the model into two segments. This violates the boundary conditions of the analysis scheme and the program terminates, printing the stresses, strains and displacements accumulated just prior to total failure. On the other hand, if successive adjustment load application results in no further element failures, the

next full load increment is read into the program, added to the accumulated load, which now reflects a "ratioed" load increment, and the anlysis continues as it did before element failure, i.e., if no elements fail, another load increment is applied, or if failures occur, the entire crack propagation procedure outlined above is repeated.

3.4 DEVELOPMENT OF THE BROKEN FIBER, LONGITUDINAL SECTION MODEL

There are two primary reasons for the development of a longitudinal model. One is to permit study of localized stress concentrations, the resulting elastic-plastic behavior of the aluminum matrix, and subsequent crack propagation in the area of boron fiber flaws. Another is to characterize the load carrying capability of a flawed boron fiber as a function of distance from the location of the fiber flaw.

These two considerations lead to the most important aspects of designing the longitudinal model, i.e., geometry, finite element grid resolution, boundary conditions in the vicinity of a flaw, and spacing of the boron fibers in the model. The problem of fiber spacing will be discussed first.

A typical cross section of a unidirectional, square array, boron/aluminum composite as shown in the figure below, the section being perpendicular to the fiber axes. A longitudinal finite element model attempts to represent the composite in a plane oriented perpendicular to this section. A longitudinal model of a section parallel to the x or y axes, through the centers of the fibers, would be representative of the minimum distance between fibers. A section cut at 45° to the x-axis and through the fiber centers would depict a maximum fiber spacing situation. When one of these fibers is broken, the load it carries decays to zero at the

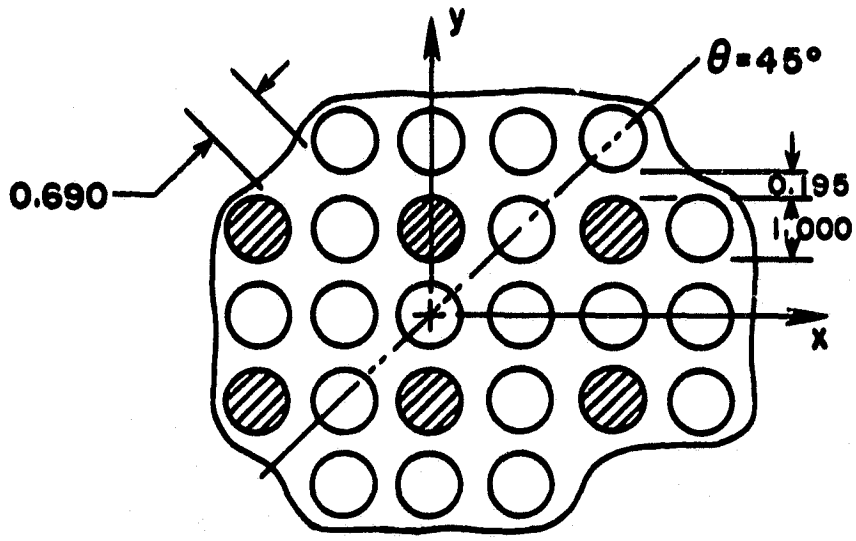

Cross Section of a Square Array of Fibers,
55 percent Fiber by Volume

broken surface, assuming that the boron-aluminum interface remains intact. At the flaw site, the fibers adjacent to the broken fiber, and to some extent the surrounding aluminum matrix, must absorb the load that the broken fiber would have otherwise carried. The aluminum transfers this excess load back into the broken fiber via a shear mechanism so that at some distance from the fiber break, that fiber is again fully effective in carrying load. It is logical to presume that the amount of aluminum between the boron fibers will have an effect on this load transfer mechanism. To characterize the effects of variation in fiber spacing, two longitudinal models were studied, one representing a 90° section cut of the transverse cross section, and another representing a 45° section cut. These two models are shown in Figures 3.6 and 3.7. Note that the fiber diameter dimensions have been normalized to unity. In Figure 3.7 the effect of the 90° section cut in diminishing the amount of local aluminum matrix is shown quite clearly. The size and aspect ratios of the fiber elements are

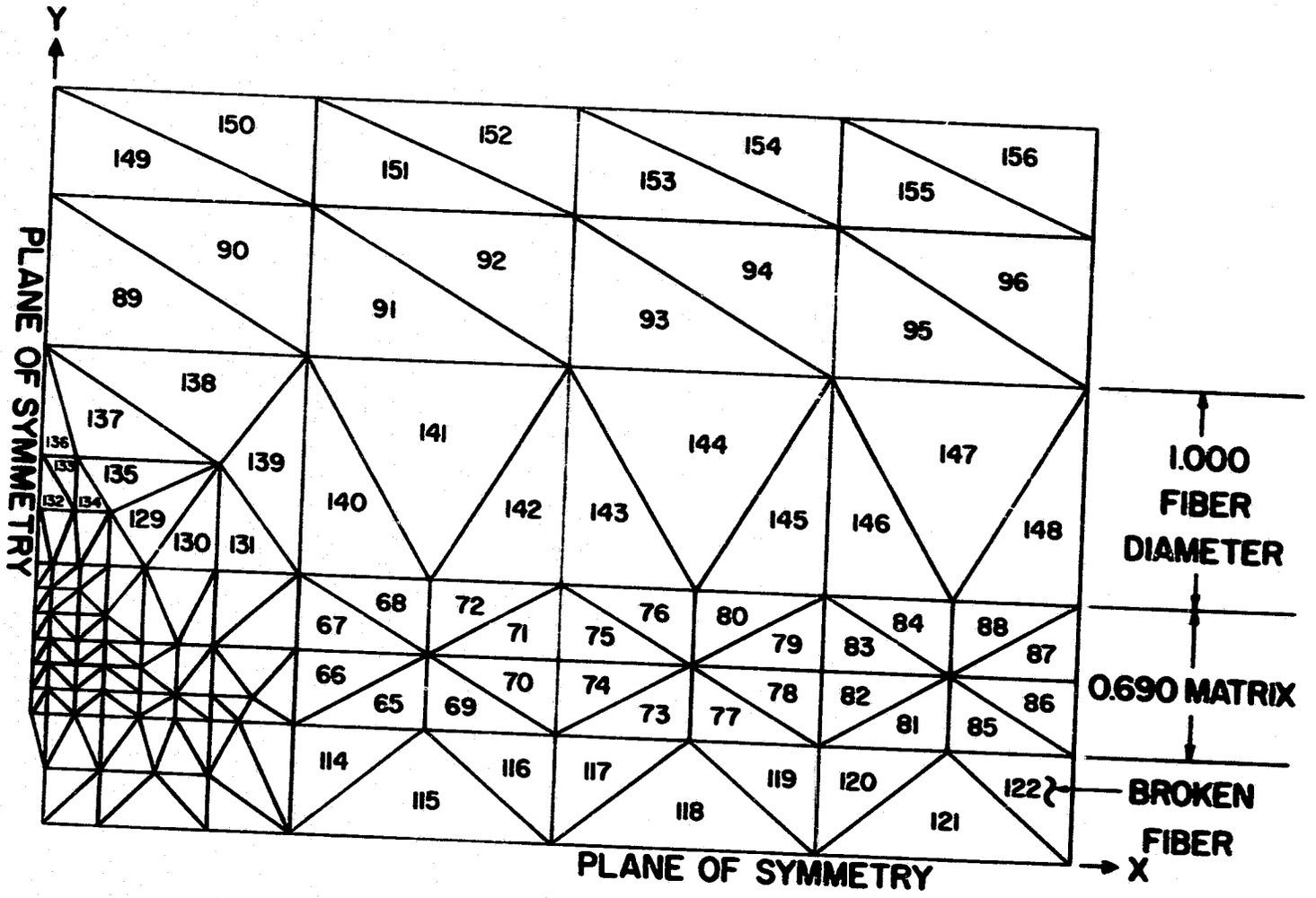

FIGURE 3.6

45° Section Longitudinal Finite Element Model with Discontinuous Boron Fiber
(See Figure 3.8 for Element Numbers in Vicinity of the Discontinuous Fiber)

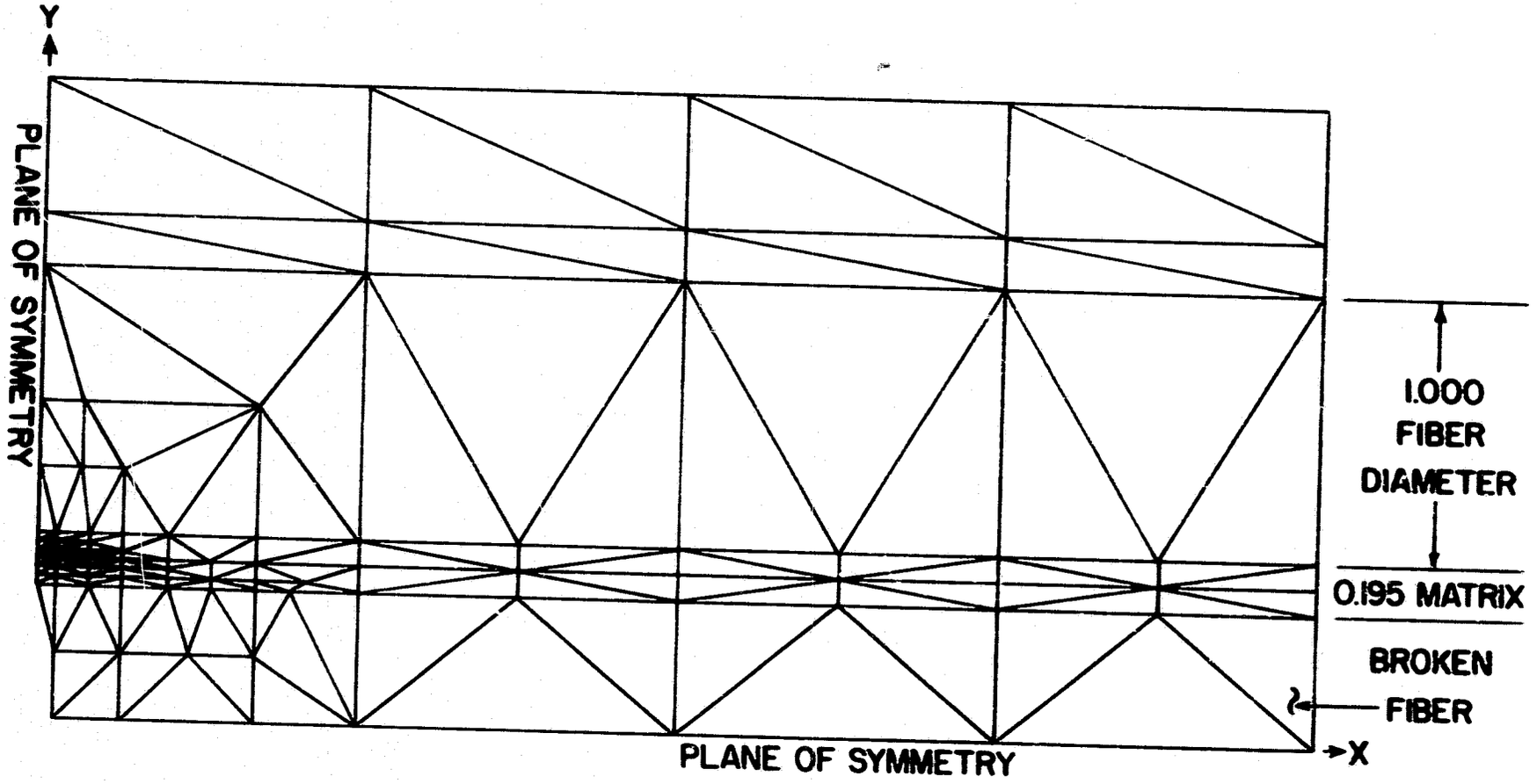

FIGURE 3.7

90° Section Longitudinal Finite Element Model with Discontinuous Boron Fiber

exactly the same as those of Figure 3.6, but the aluminum elements of the 90° section model are so compressed that the element numbers, which are identical to those of Figure 3.6 have been eliminated for clarity.

The second problem that must be solved in the finite element modeling of a broken fiber in a composite is the geometry in the area of the fiber discontinuity-matrix interface. The efforts of the present investigators to resolve this problem have been evolutionary in nature and were described in detail in Section 5.2 of Reference [23].

The results of this evolutionary process are the finite element models shown in Figures 3.6 and 3.7. Some of the features of this model can be illustrated by referring to Figure 3.8, a section of the model representing the discontinuous fiber and the local aluminum matrix. Note that the free surface of the discontinuous boron fiber is extended out to the model's plane of symmetry by the addition of fiber element number 157. Longitudinal models run without this element developed extremely high stress levels in aluminum element number 1 at very low levels of applied load. While this situation might occur in a boron/aluminum composite if the fiber were discontinuous and its ends separated by some finite amount at the time of fabrication, it was felt that the present configuration, as shown in Figure 3.8, was of more general use. This configuration might be used to represent a fiber that has broken during fabrication, or, if flawed locally, failed at a very low loading of the unidirectional composite. Note the small size and uniformity of the aluminum elements in the area of the end of the discontinuous fiber. This is to permit a closer approximation of actual crack growth, as discussed in Section 3.3. In order to prevent the broken fiber from having any load capability at $x = 0$, node point 12 has been relased from its x-direction fixity. This results

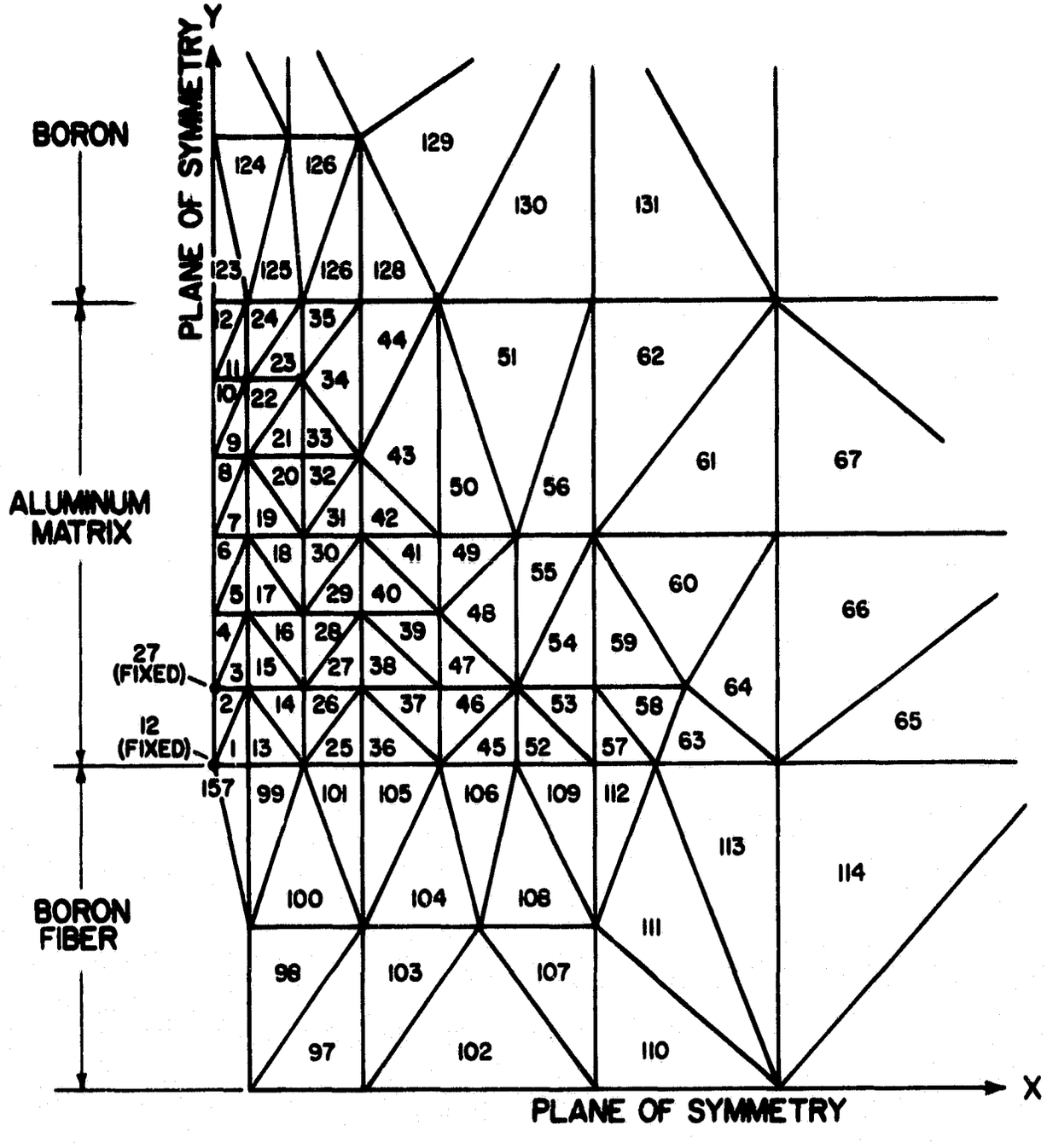

FIGURE 3.2

Finite Element Modeling of the Discontinuous Fiber

in a free surface for element 2 along the y-axis, or in other words, an initial crack in the aluminum as might actually occur from the initial release of energy caused by the fiber failing at a low load level.

3.5 DEVELOPMENT OF THE TRANSVERSE SECTION MODEL

Finite element modeling of a transverse section of a unidirectional boron/aluminum composite is fairly straightforward. However, the need to study the influence of a reduced load capacity in one fiber on its neighboring fibers requires that a minimum section model such as that shown in Figure 3.9 be employed. This model represents the first quadrant of a repeating unit cell of a rectangular array of fibers. In effect, a flawed fiber can be considered to be surrounded by eight other fibers in the array. A model of this type can easily lead to a great number of elements, and attempting to increase the resolution of the grid at selected locations often results in a very large bandwidth of the overall stiffness matrix for the finite element model. The transverse model developed and reported in the First Quarterly Report [22], proved to be too large for the University of Wyoming's present computer. This resulted in the development of the model shown in Figure 3.9. Also, during the last year, the micromechanics analysis computer program has been modified to permit the inclusion of as many as four different materials, each having different properties. This capability is essential in representing breaks or flaws in the boron fibers of a transverse model via reduced stiffness.

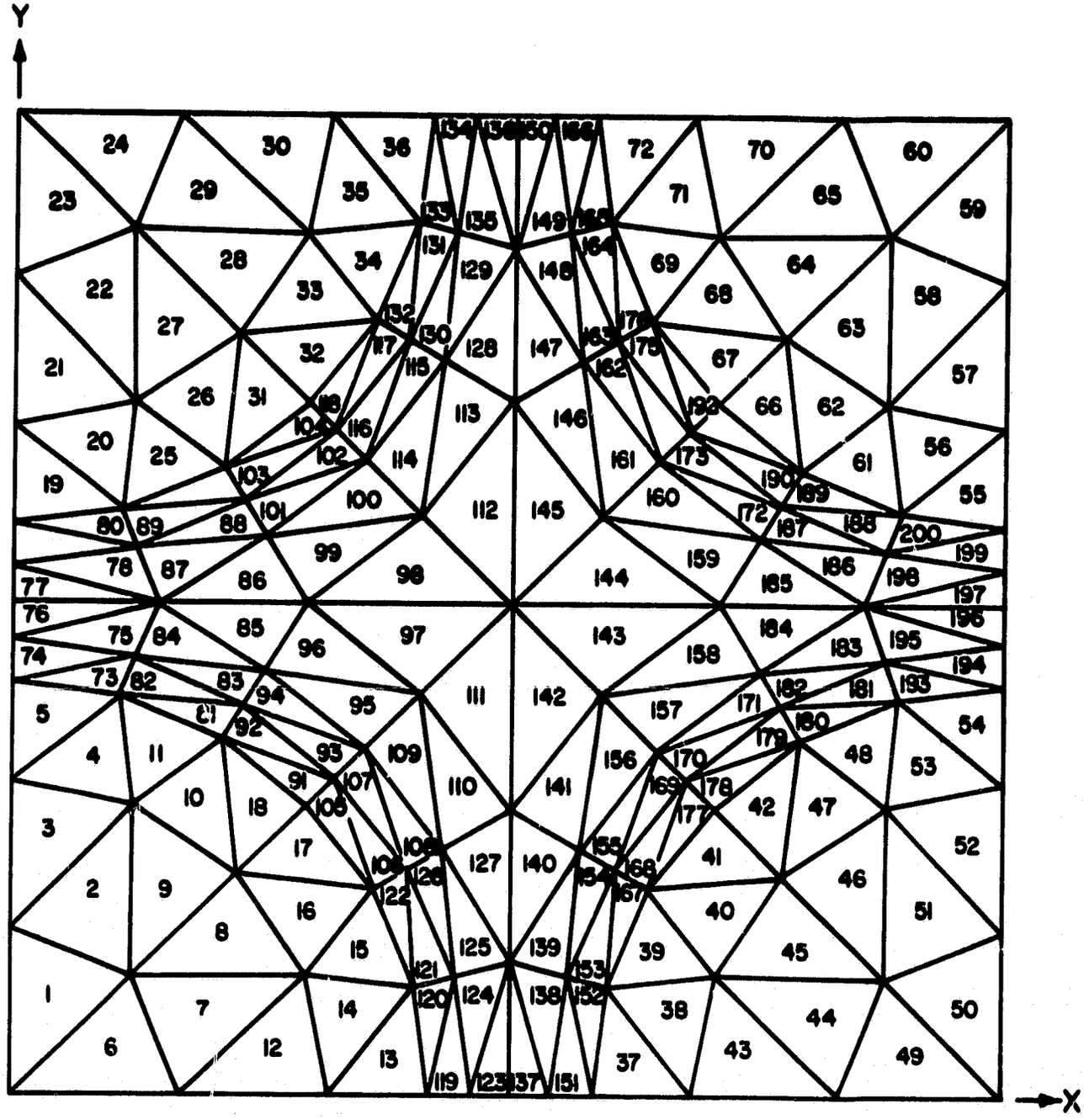

FIGURE 3.9

Transverse Section Finite Element Model,
55 Percent Fiber by Volume

SECTION 4

MATERIAL PROPERTIES

In modeling the boron/aluminum composite, the boron fibers have been treated as brittle, linearly elastic materials with isotropic strength and stiffness properties. The aluminum matrix has also been considered to be isotropic, but is modeled as an elastoplastic material. To accomplish this, the actual stress-strain curve of the aluminum alloy selected is input to the analysis by curve fitting via a Richard-Blacklock two-parameter equation, as discussed in Section A.5. Thus, at any load level the tangent modulus for any given element can be computed. This makes possible an accurate representation of the plastic deformation of the matrix.

Although the nonlinear material properties of any matrix material, e.g., another aluminum alloy, can readily be incorporated in the analyses, a 6061-T6 aluminum alloy at 75°F was chosen for the initial studies. The material properties shown in Table 4.1 were obtained from Reference [24]; the full range stress-strain curve for determining the curve fit parameters used is shown in Figure 4.1.

TABLE 4.1

Aluminum Matrix Material Properties - 6061-T6 Alloy [24]

Young's Modulus	$E = 10.0 \times 10^6$ psi
Poisson's Ratio	$\nu = 0.33$
Tensile Yield Strength	$F^{ty} = 36000$ psi
Tensile Ultimate Strength	$F^{tu} = 45000$ psi
Coefficient of Thermal Expansion	$\alpha = 13.0 \times 10^{-6}$ in./in./°F

The boron fiber properties indicated in Table 4.2 were obtained from Reference [25].

TABLE 4.2

Boron Fiber Material Properties [25]

Young's Modulus	$E = 60.5 \times 10^6$ psi
Poisson's Ratio	$\nu = 0.130$
Tensile Strength	$F_{tu} = F_{ty} = 500{,}000$ psi
Coefficient of Thermal Expansion	$\alpha = 9.0 \times 10^{-6}$ in./in./°F
Ultimate Strain	$\epsilon^{tu} = \frac{F_{tu}}{E} = 8264 \times 10^{-6}$ in./in.

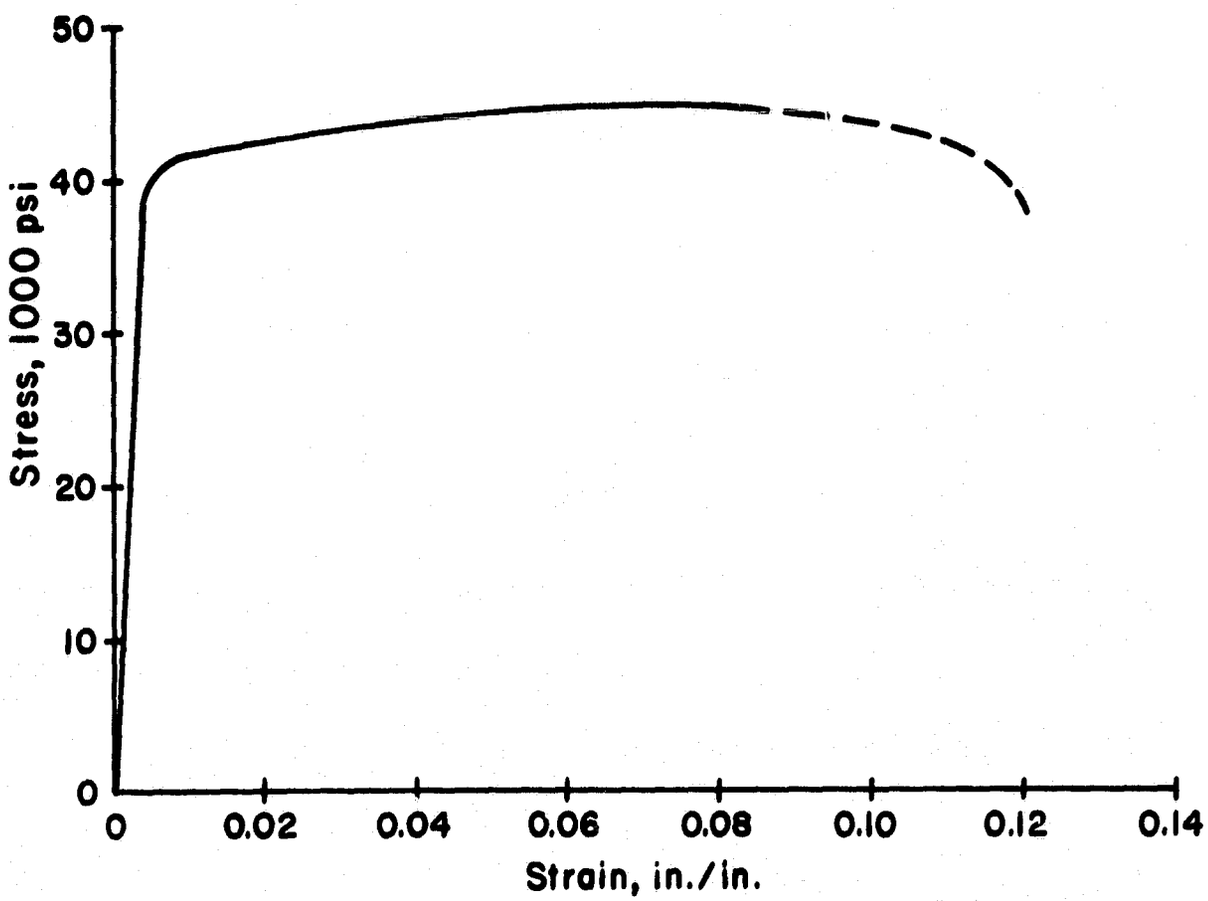

FIGURE 4.1

Typical Full Range Stress-Strain Curve For
6061-T6 Aluminum Alloy at Room Temperature [24]

SECTION 5

NUMERICAL RESULTS

The introduction of crack initiation and growth capability to the micromechanics program has made possible a much more extensive study of the effects of a discontinuous fiber in a boron/aluminum composite. However, a numerical difficulty was revealed in the crack propagation procedure shortly before the end of this report period. Debugging of the subsequent corrected computer program has prevented the presentation of the crack growth results in this report; they will be presented in full detail in the next quarterly progress report. In spite of this difficulty, the results of loading both the 45° section and the 90° section models to the point of first element failure are available, and very informative significant differences in the load carrying capability of the 45° section model versus the 90° section model have been revealed. It is anticipated that future analyses with crack propagation will generate even more important insights concerning the generalized plane strain treatment of this problem.

The 45° section model and the 90° section model, as described in Section 3.4, represent a unidirectional composite with 25 percent of the fibers containing a break. Larger models with more unbroken fibers can easily be studied if desired. Each of these models has been loaded to the point of crack initiation (first element failure), and the difference in load capability of each at this point is considerable. In both cases, initial plastic deformation occurs at very low load levels, and due to considerable plastic strain capability of the aluminum matrix, as shown

in Figure 4.1, the loading increments beyond that point are kept very small, i.e., 1000 to 3000 psi. Considerable localized plastic deformation was developed in the region of the fiber discontinuity before an element failure occurred. This in turn generally triggered the failure of several more matrix elements before another loading increment could be applied. In the paragraphs that follow, the results of loading the 45° section and the 90° section longitudinal models up to the point of crack initiation will be studied. In Section 5.3, the results of axial loading of the transverse model and simulation of a broken fiber are reviewed.

5.1 AXIAL LOADING OF THE 45° SECTION LONGITUDINAL MODEL

The 45° section longitudinal model, as illustrated in Figure 3.6, was loaded in the direction of the fiber axes (x-direction) to a level of 66,076 psi average applied stress, at which point element number 2 failed. Initial plastic deformation was also observed in element number 2, at an average applied stress level of 17,000 psi. Plastic deformation, in this analysis, is defined as the point at which the octahedral shear stress-octahedral shear strain curve becomes nonlinear. For the 6061-T6 aluminum alloy used in this study, the octahedral shear yield strength is 16,970 psi. Element number 2 would be the first to experience plastic deformation, for the reasons cited in Section 3.3.

Loading was increased monotonically until element number 2 failed, at an average applied stress level of 66,076 psi. At this level there was considerable plastic deformation in the region of the fiber discontinuity, with several elements adjacent to number 2 very near failure. By using the plotting capability of the micromechanics computer program, this zone of plastic deformation at the point of imminent failure of element

number 2 can be seen. In Figure 5.1, contours of constant octahedral shear stress for the aluminum matrix have been plotted on an outline of the 45° section finite element model. Note that the contour values are for octahedral shear stresses normalized with respect to the yield strength, 16,970 psi. This means that any area enclosed by contour lines that are greater than or equal to one has been plastically deformed. As Figure 5.1 shows, considerable plastic deformation has occurred at the 66,000 psi applied stress level. In addition, similar contour plots for octahedral shear strain, maximum principal stress, minimum principal stress, and in-plane shear stress (τ_{xy}) are provided in Figures 5.2, 5.3, 5.4, and 5.5, respectively. These illustrate very well the general state of stress in the aluminum matrix at the load level of imminent crack initiation.

A study was also made of the loading intensities in the boron fibers at various load levels, in an attempt to further understand the mechanisms of load transfer to the discontinuous fiber as plastic deformation increases. In Figures 5.6 and 5.7, the relative loading intensities of the three boron fibers in the model are compared as a function of the axial distance from the flaw site. The two load levels chosen are 16,000 psi for Figure 5.6 and 66,000 psi for Figure 5.7. From these figures it can be seen that the end of the broken boron fiber carries no axial stress, as it must, and that the load level in the adjacent fiber rises abruptly in the vicinity of the fiber break. Of particular interest is the relative loading of the discontinuous fiber as the load level increases. It will be noted that the slope of the load curve for the discontinuous fiber at the flaw site decreases as the applied load increases. In addition, at an applied stress level of 16,000 psi, the broken fiber has attained a stress level 78 percent that of a remote fiber at 4.55 fiber diameters from the

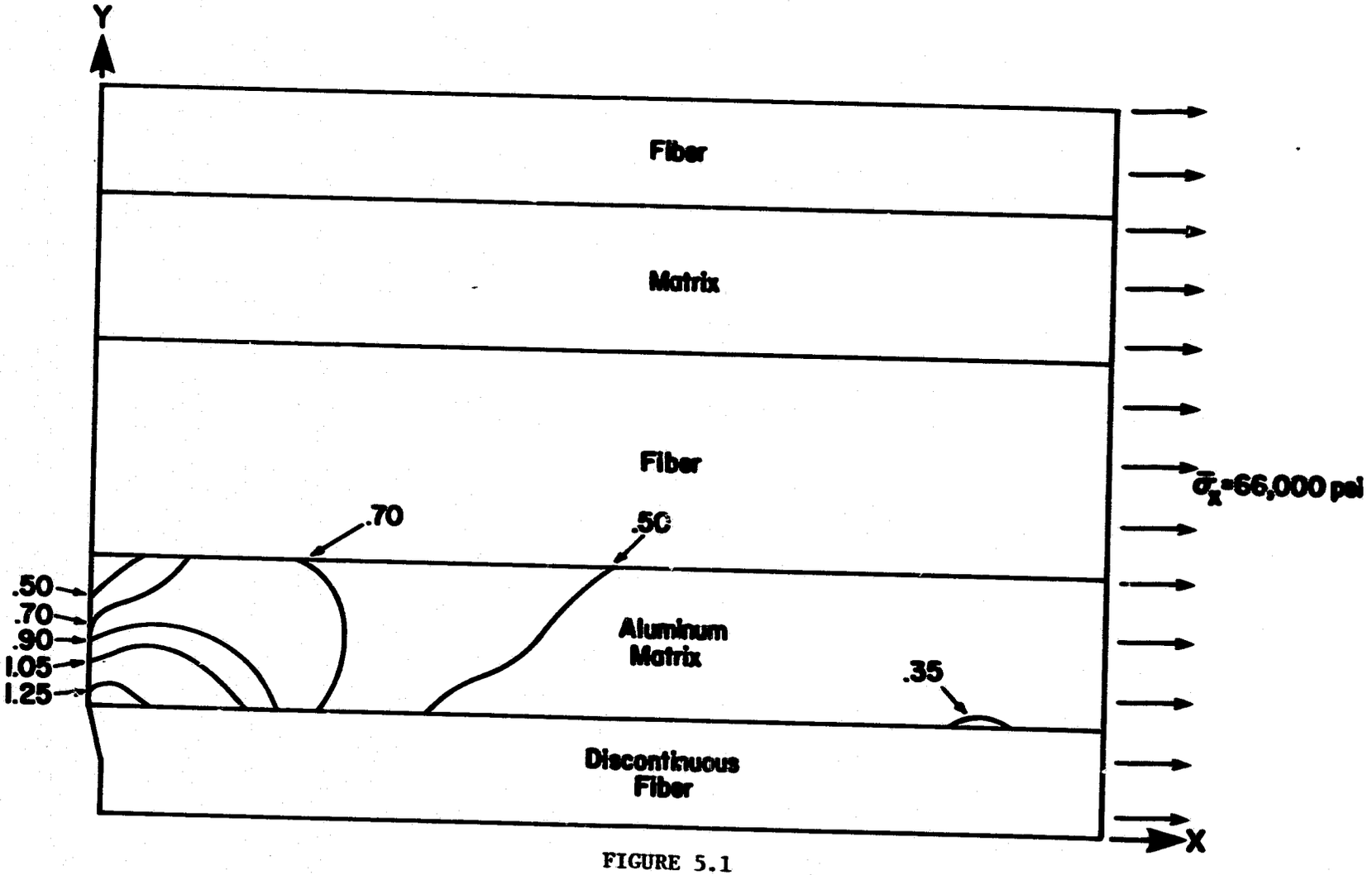

FIGURE 5.1

Normalized Octahedral Shear Stress Contours Just Prior to Crack Initiation (Applied Stress = $\bar{\sigma}_x$ = 66,000 psi), 45° Section Longitudinal Model, 55 Percent Fiber by Volume, (Normalized by Dividing by the Matrix Yield Stress, i.e., 16,970 psi).

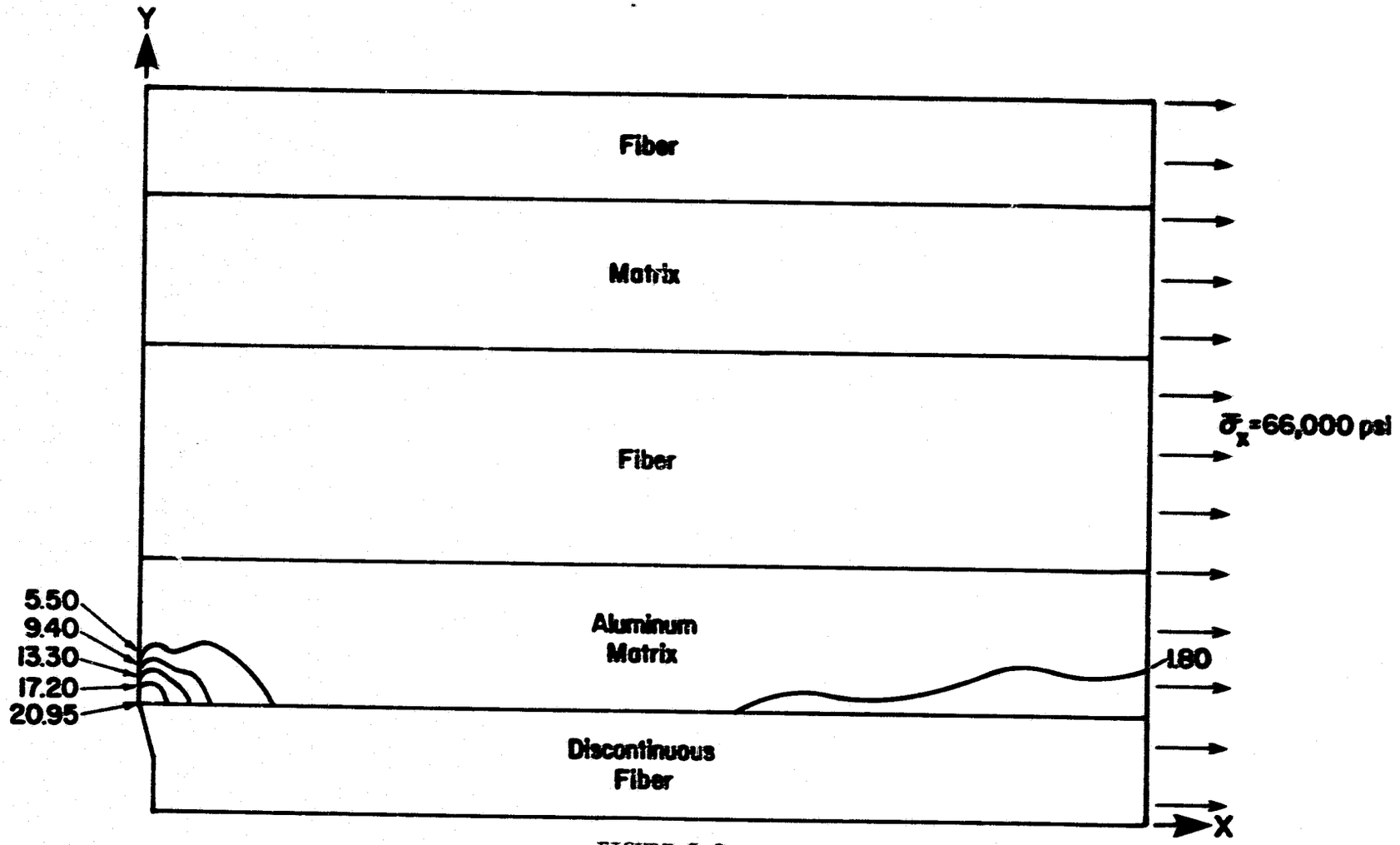

FIGURE 5.2

Octahedral Shear Strain Contours Just Prior to Crack Initiation, 45° Section
Longitudinal Model, ksi

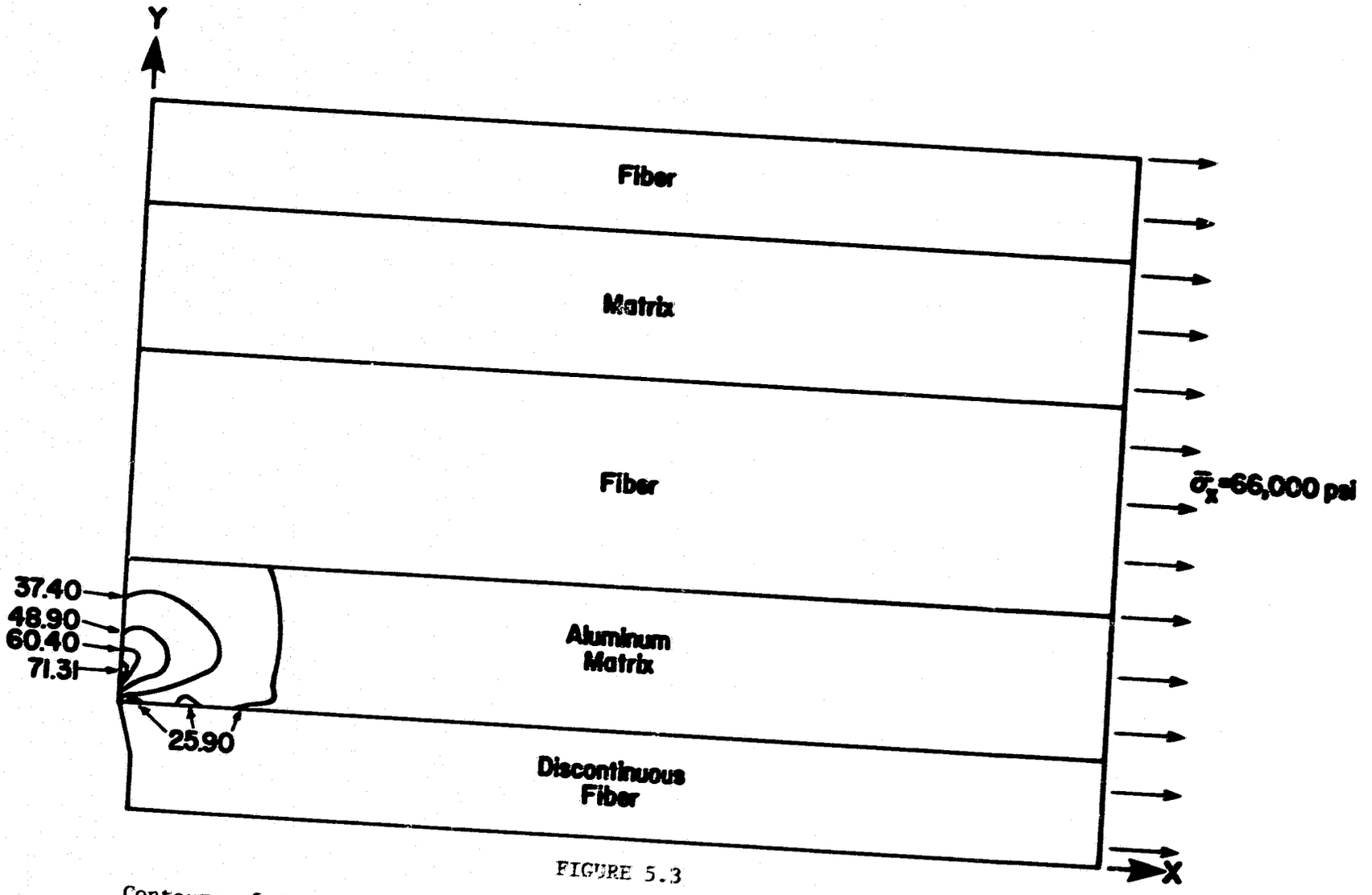

FIGURE 5.3

Contours of Constant Maximum Principal Stress Just Prior to Crack Initiation, 45° Section Longitudinal Model, ksi

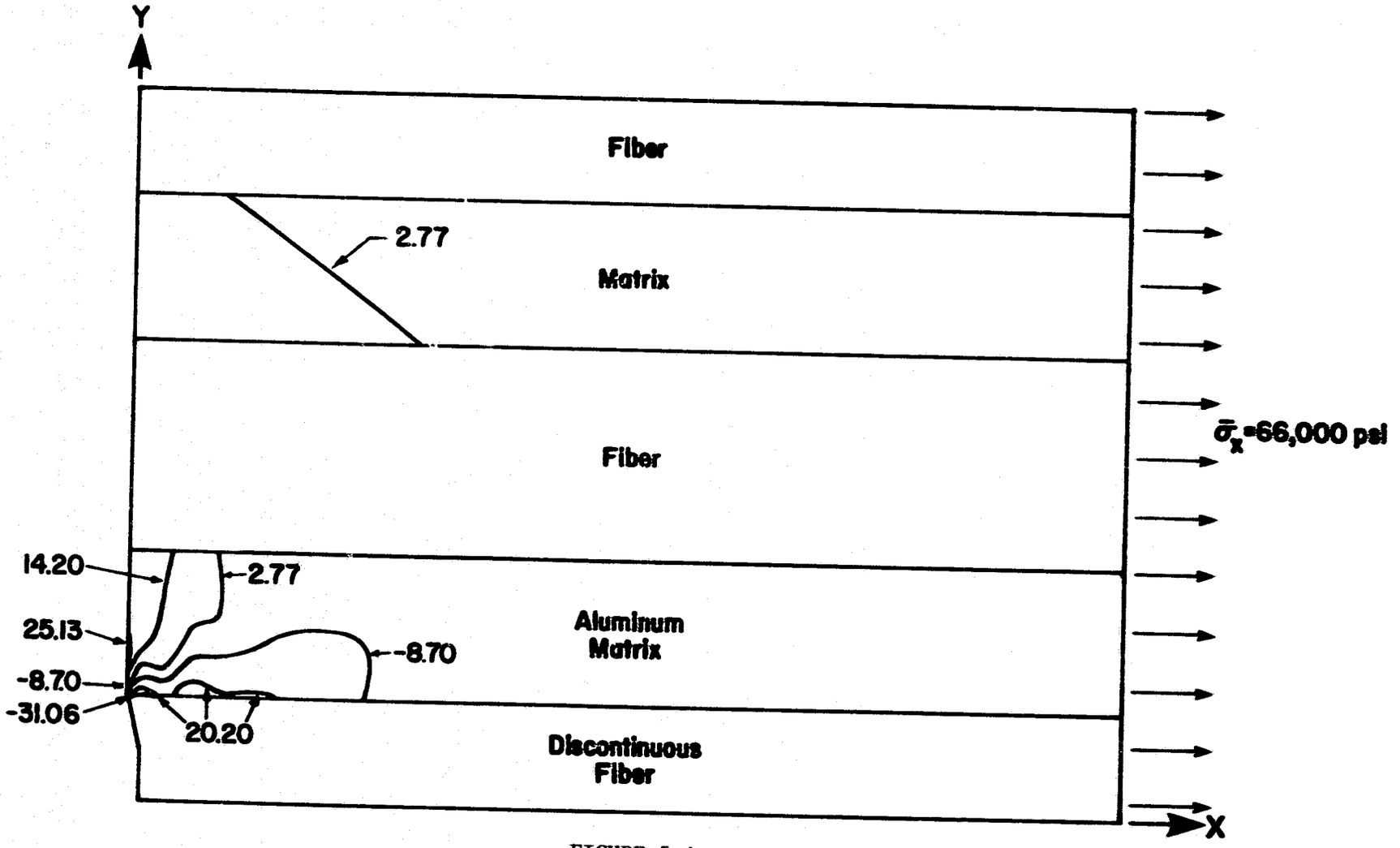

FIGURE 5.4

Contours of Minimum Principal Stress Just Prior to Crack Initiation,
45° Section Longitudinal Model, ksi

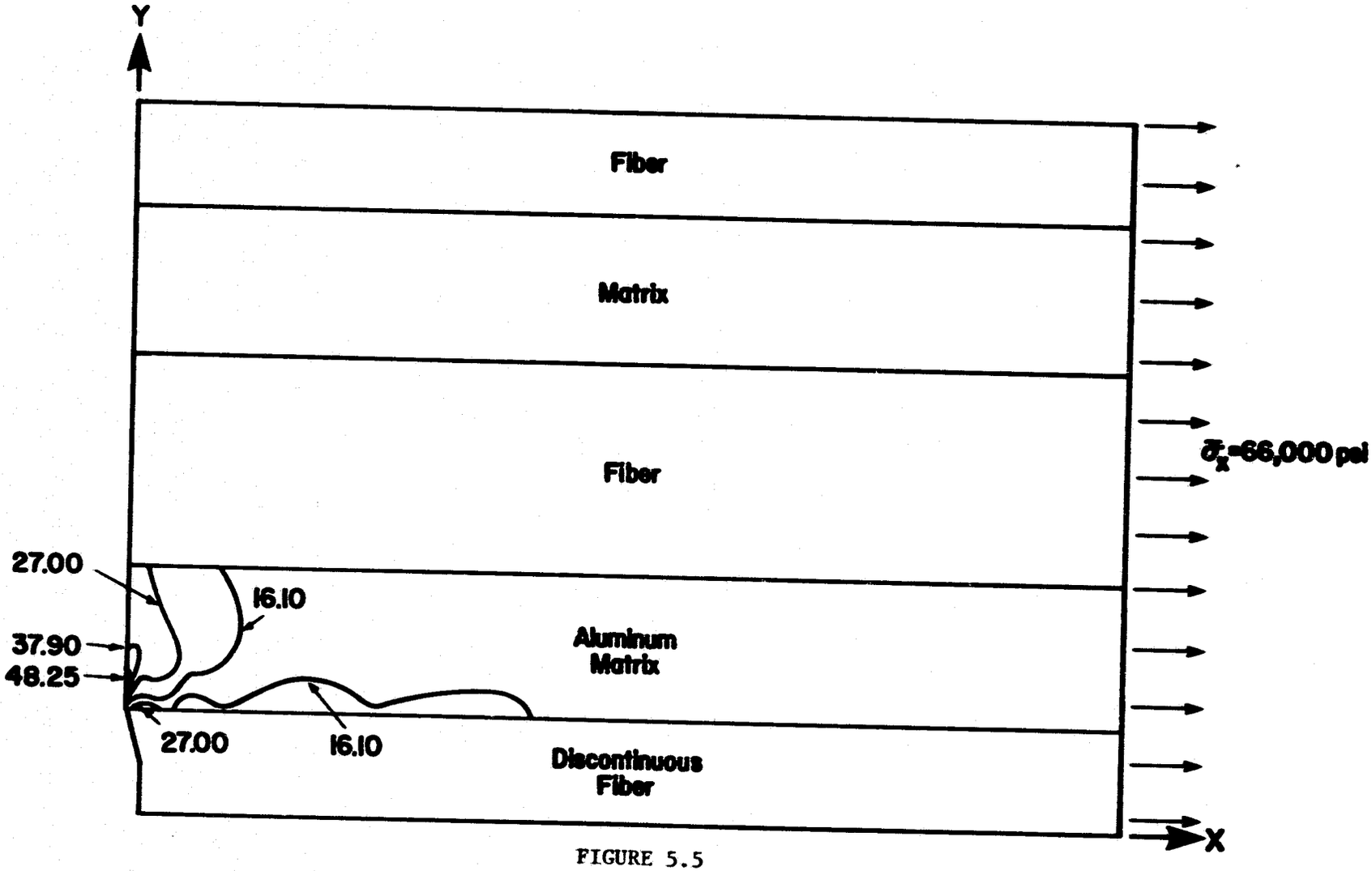

FIGURE 5.5

Contours of In-Plane Shear Stress Just Prior to Crack Initiation 45° Section Longitudinal Model, ksi

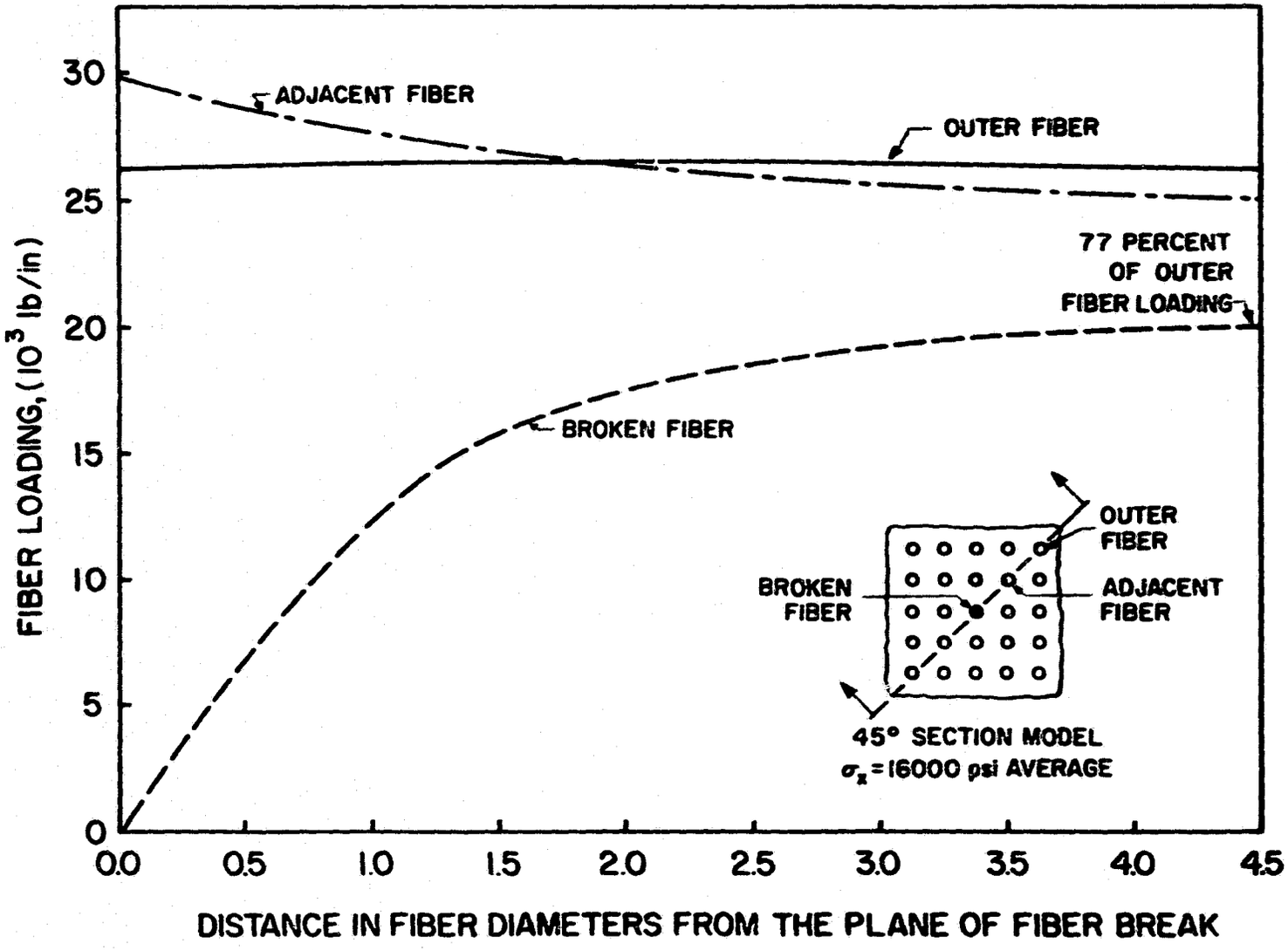

FIGURE 5.6

Fiber Loading Versus Distance From the Broken Fiber, 45° Section Model, 16,000 psi Average Applied Stress

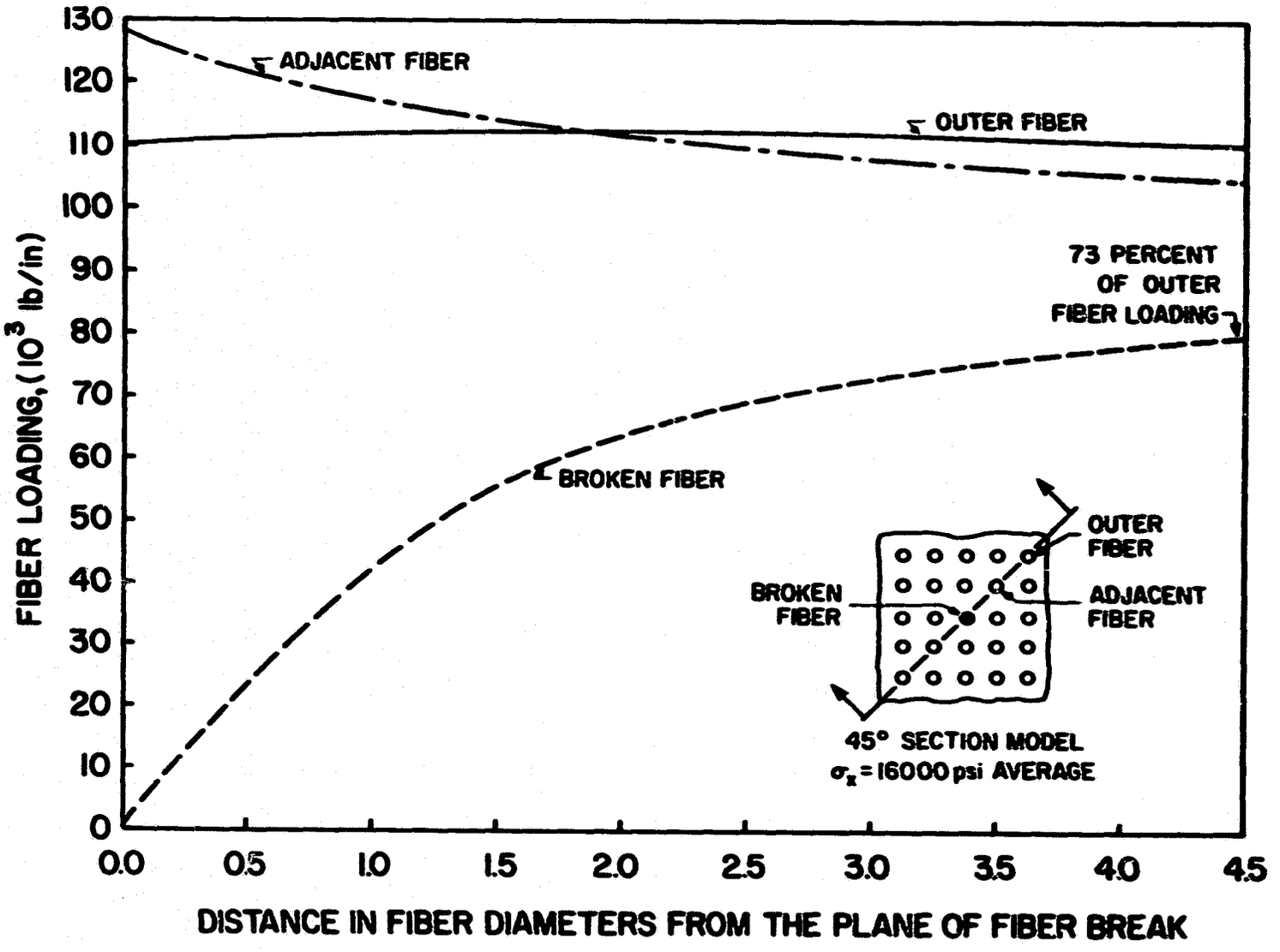

FIGURE 5.7

Fiber Loading Versus Distance From the Broken Fiber Surface, 45° Section Model, 66,000 psi Average Applied Stress

flaw site, while at an average applied stress level of 66,000 psi, the broken fiber has been loaded to only 73 percent at 4.55 fiber diameters. These values imply that at a sufficiently large distance from a flaw site, all the boron fibers will be equally loaded, but that the distance required for this condition to exist increases as the average stress level increases. Crack propagation will no doubt cause the distance from the crack at which the broken fiber is again fully loaded to be much greater still.

As an illustration of the energy absorption capacity of the 45° section broken fiber longitudinal model, the composite stress versus composite strain has been plotted up to the point of crack initiation, as shown in Figure 5.8. It will be noted that the curve is essentially linear, in spite of the considerable plastic deformation shown in Figure 4.1. This is due to the fact that the boron fibers, whose axial modulus is very much higher than that of the aluminum, are essentially linear in their stress-strain response. In fact, even at the plane of fiber discontinuity, the boron fibers are carrying 76 percent of the applied load. At two fiber diameters from that plane, 90 percent of the applied load is being carried by the boron fibers. The overall stiffness of the 45° section model, i.e., the shape of the stress-strain curve as shown in Figure 5.8, proved to be 36.0×10^6 psi, or about 60 percent of the axial stiffness of the boron fibers.

5.2 AXIAL LOADING OF THE 90° SECTION LONGITUDINAL MODEL

In loading the 90° section longitudinal model, Figure 3.7, parallel to the boron fiber axes, plastic deformation was first observed in element number 2 at an applied average stress level of just under 10,000 psi. This

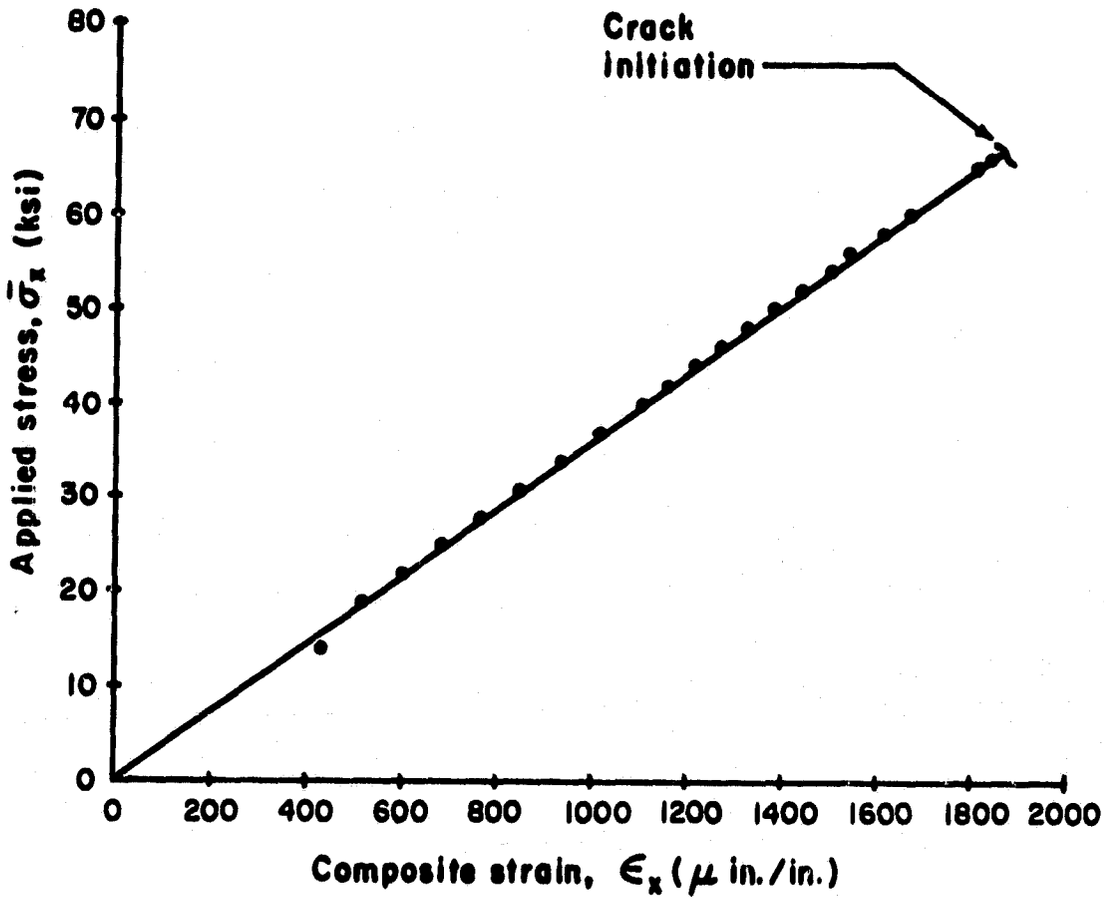

FIGURE 5.8

Plot of Applied Stress Versus Composite Strain
for the 45° Section Longitudinal Model

is substantially lower than the 16,000 psi level that was necessary to cause plastic behavior in the 45° section model, and is due primarily to the fact that the apparent volume of aluminum matrix available to transmit load between the discontinuous and intact boron fibers is only about 30 percent of that seen by the 45° section model.

Loading of the 90° section model was increased until element number 2 exhausted its strain energy capacity at 40,150 psi applied stress. Again,

stress and strain contour plots were generated for the load level which was reached immediately prior to the first failure, and these are shown in Figures 5.9, 5.10, 5.11, 5.12, and 5.13 for the normalized octahedral shear stress, octahedral shear strain, maximum and minimum principal stresses, and the in-plane shear stress, respectively. It will be noted that the zone of plastic deformation, as defined by the 1.03 contour in Figure 5.9, is considerably less extensive than was observed in the 45° section model, Figure 5.1. From preliminary results of crack propagation computer runs, it is quite apparent that the pattern of deformation, flaw growth, and fiber loading differs quite significantly between the 45° and the 90° section longitudinal models. Further, the differences in load levels necessary to initiate plastic deformation and later, crack formation, for the two models indicates that the proximity of adjacent fibers to a flawed or discontinuous fiber has an important effect on the behavior of the total composite material. This problem will be discussed further in Section 6.

Another difference in the response of the 90° section model when compared with the 45° section model is shown in Figure 5.14, in which the composite stress-strain response of the 90° section model is plotted up to the point of crack initiation. The composite axial modulus of the 90° section model is found to be 49.0×10^6 psi, using Figure 5.14. This is significantly stiffer than the 45° section model, as would be expected in view of the larger boron fiber volume fraction of the 90° section model. The strain energy necessary to initiate failure in the 90° section model was determined to be 36.1 in.-lb./in., while in the 45° section model, 123.2 in.-lb./in. of energy was absorbed before crack initiation.

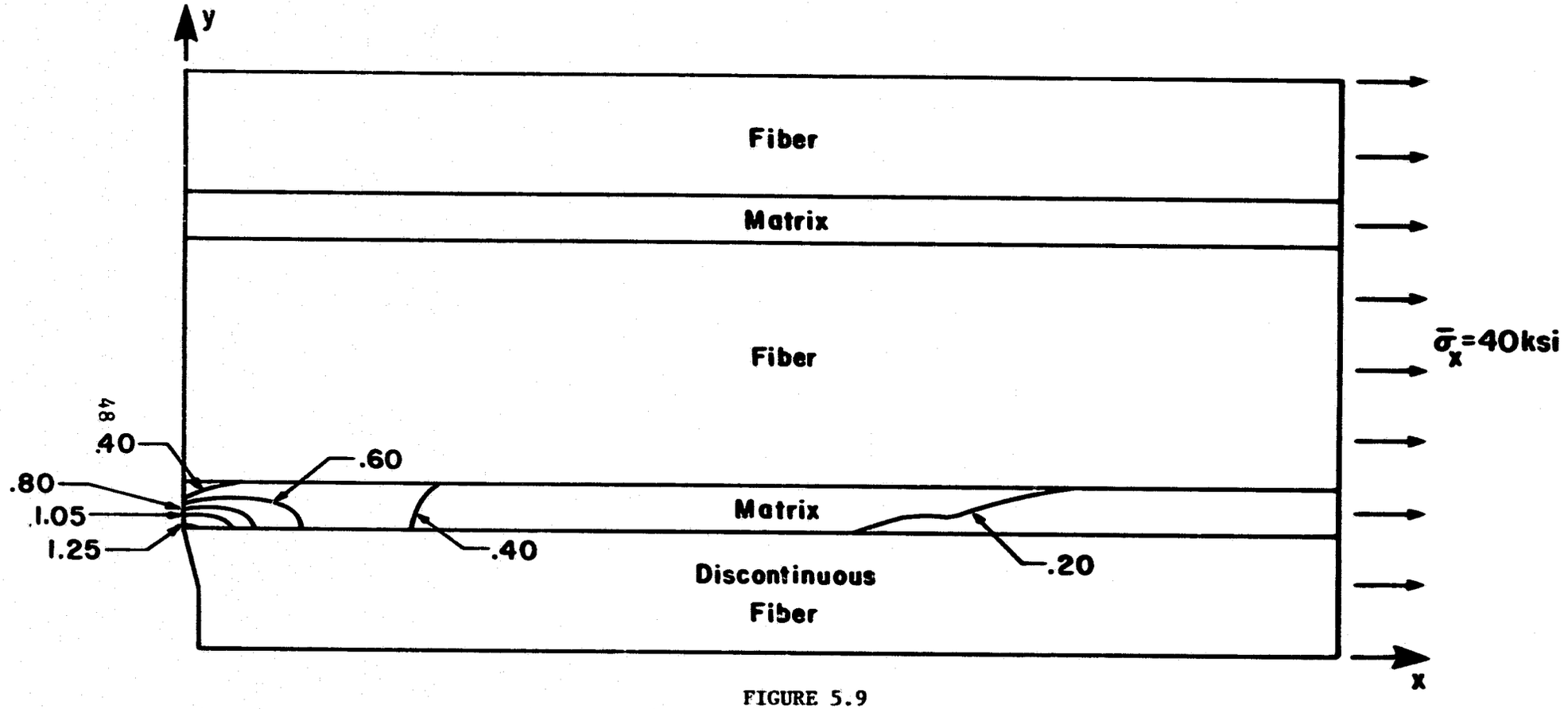

FIGURE 5.9

Contours of Constant Octahedral Shear Stress Just Prior to Crack Initiation, 90° Section Longitudinal Model (Normalized by Dividing by the Matrix Yield Value of 16,970 psi)

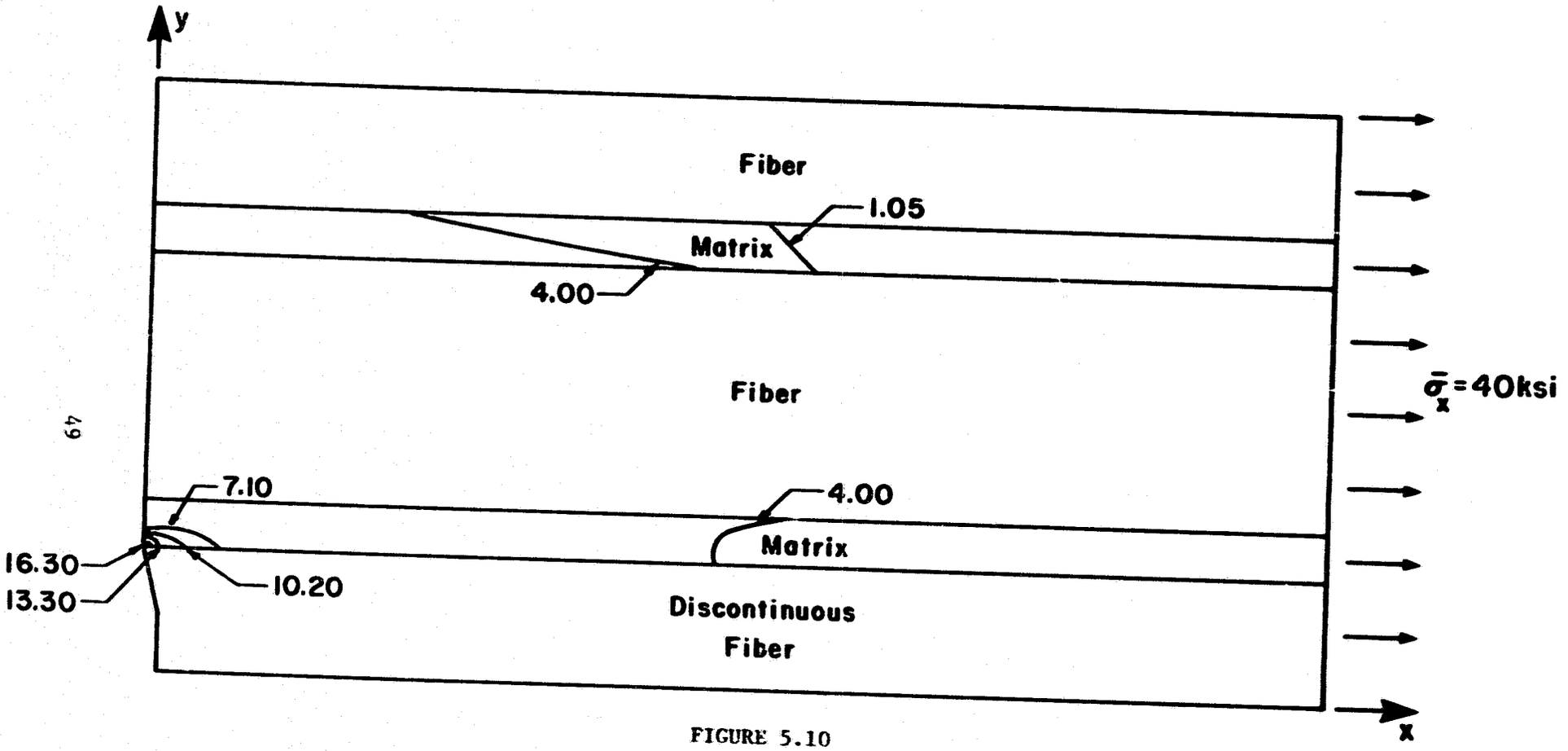

FIGURE 5.10

Contours of Constant Octahedral Shear Strain Just Prior to Crack Initiation, 90° Section Longitudinal Model (10^{-3} in./in.)

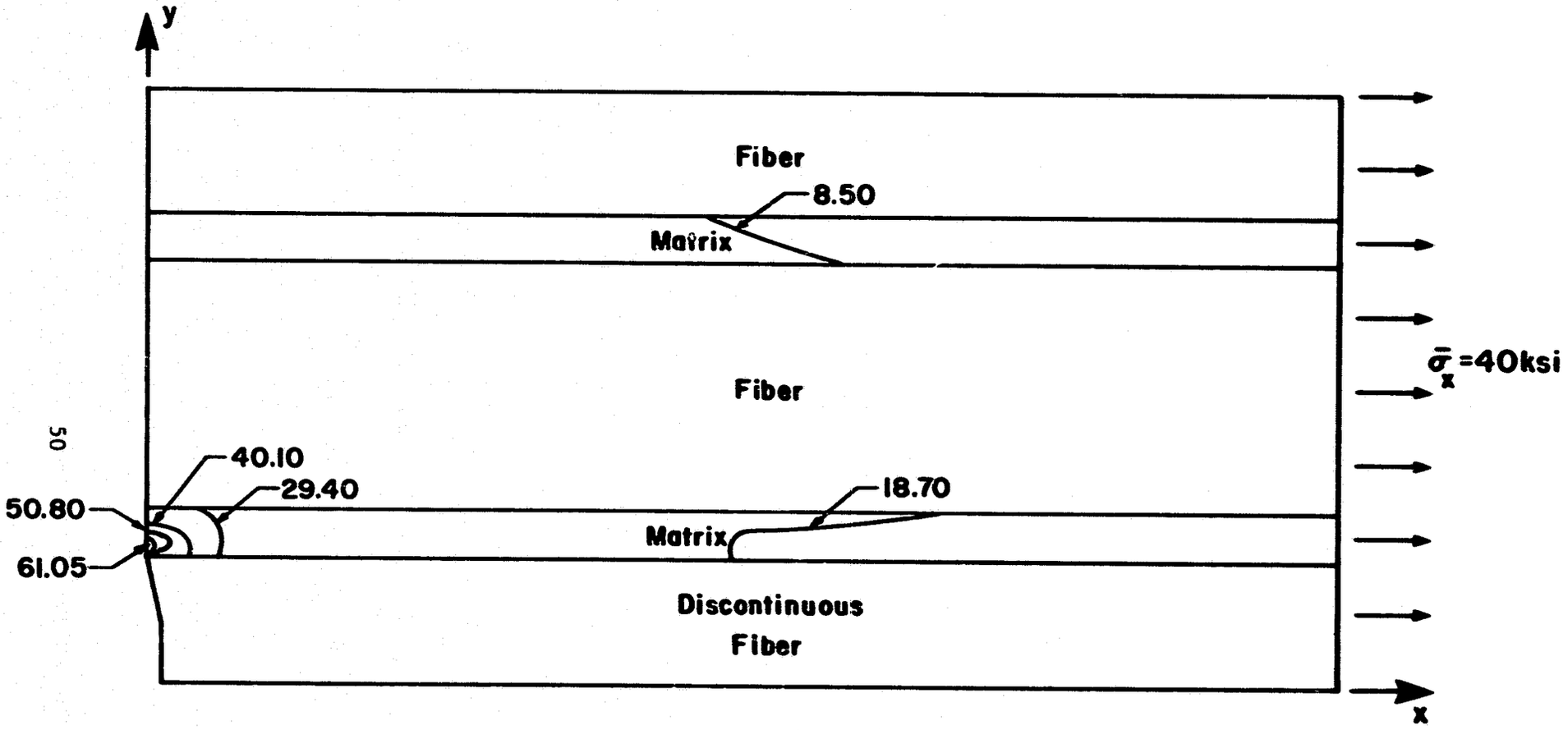

FIGURE 5.11

Contours of Maximum Principal Stress Just Prior to Crack Initiation, 90° Section Longitudinal Model (ksi)

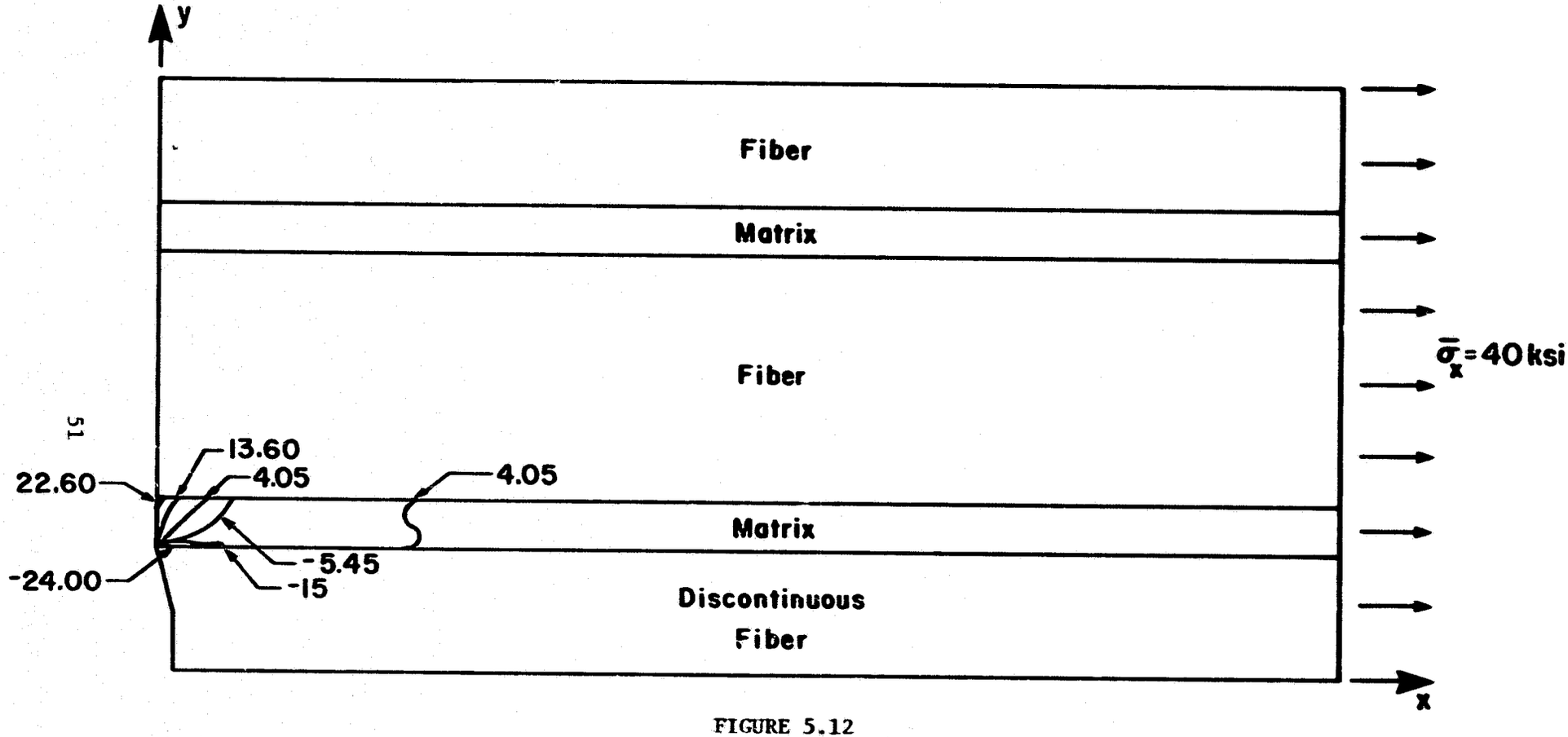

FIGURE 5.12

Contours of Minimum Principal Stress Just Prior to Crack Initiation, 90° Section Longitudinal Model (ksi)

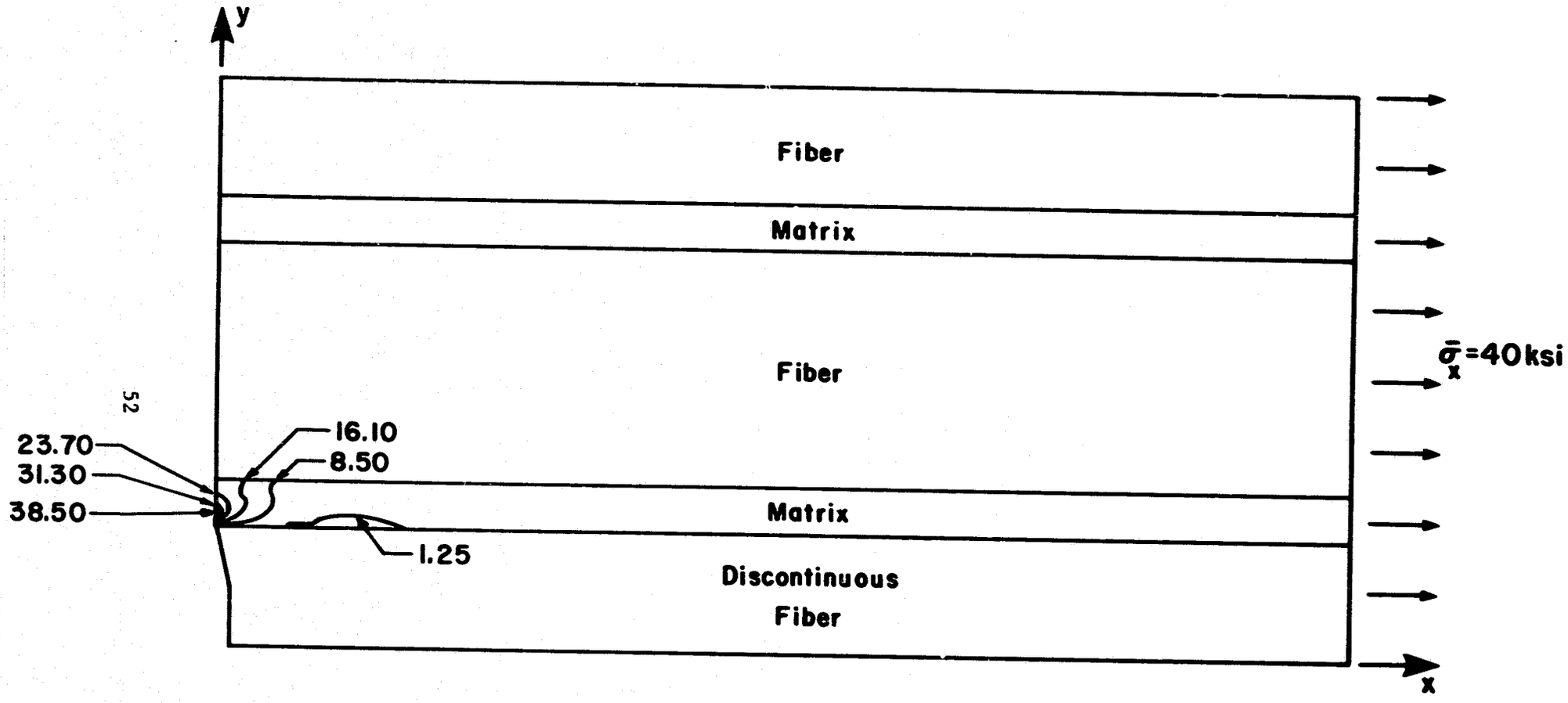

FIGURE 5.13

Contours of Constant In-Plane Shear Stress Just Prior to Crack Initiation, 90° Section Longitudinal Model (ksi)

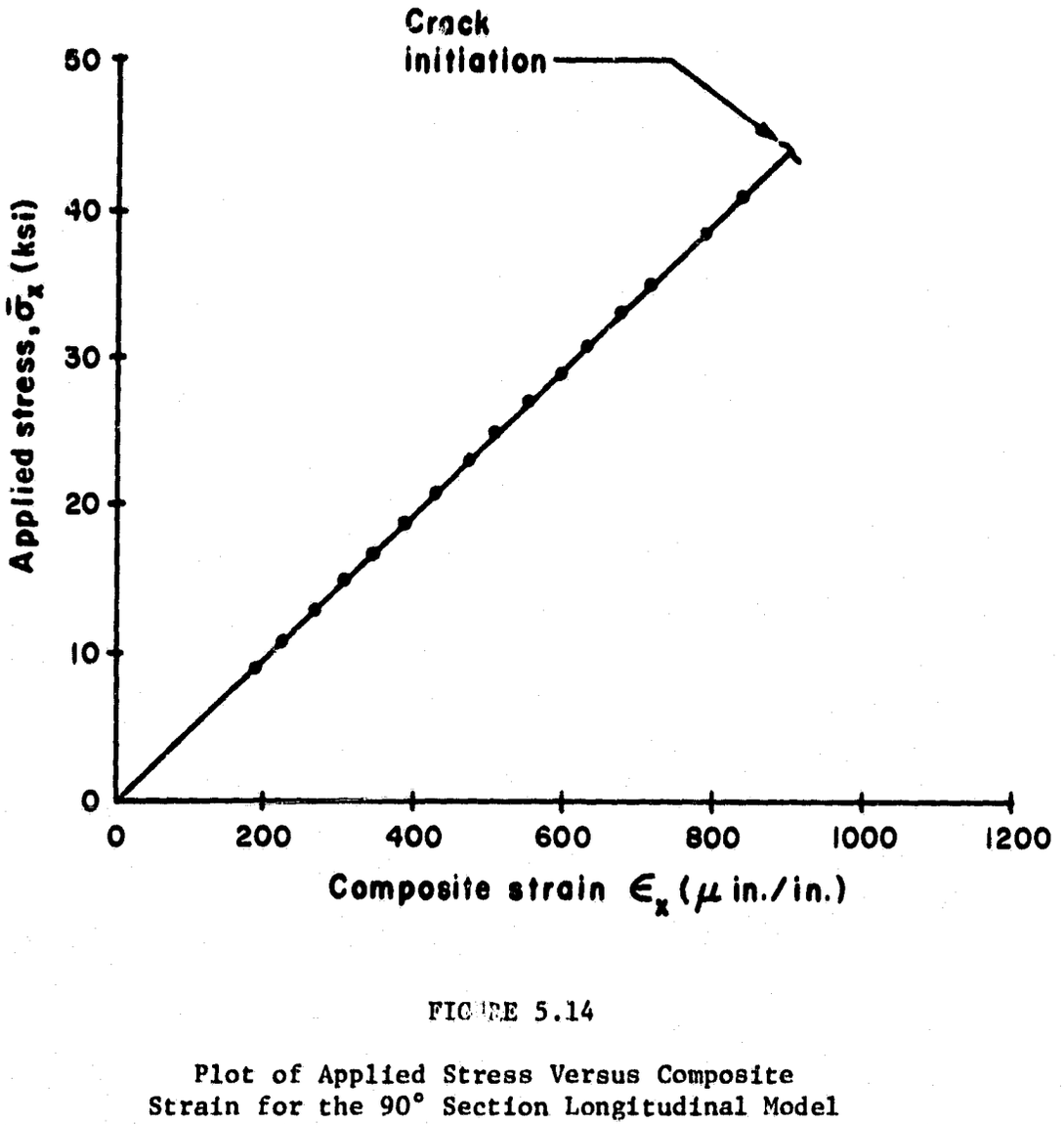

FIGURE 5.14

Plot of Applied Stress Versus Composite
Strain for the 90° Section Longitudinal Model

5.3 AXIAL LOADING OF THE TRANSVERSE SECTION MODEL

The transverse section model, as illustrated in Figure 3.9, was loaded in the out-of-plane or z-direction, both in the unflawed condition and with one broken fiber. In order to approximate the broken fiber plane of the longitudinal models, the transverse model was run with the stiffness properties of one of the fibers reduced to zero, as shown in the following sketch:

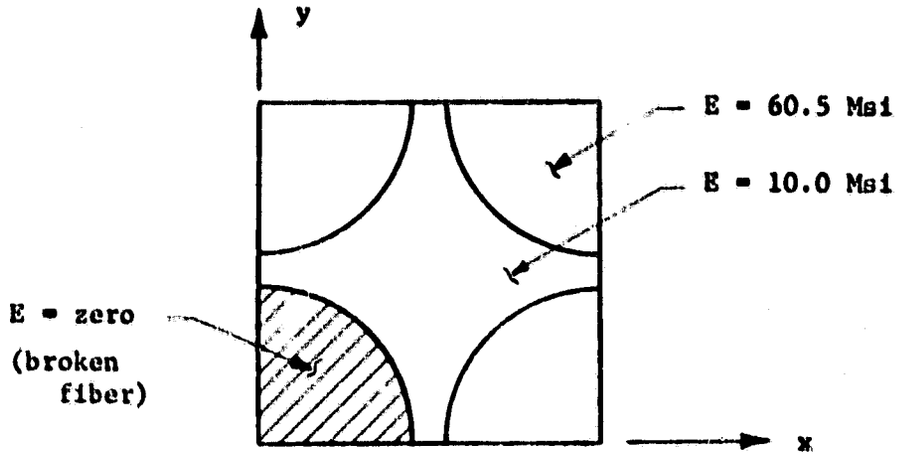

The percentage of the total load carried by the fibers of the unflawed transverse model proved to be 89.0 percent, which compares very well with the percentage of load carried by the fibers of the 45° section model, which was 89.1 percent. When the transverse model was run with one fiber deleted, it was found that the three remaining fibers carried 85 percent of the applied load, which is in good agreement with the 90° section longitudinal model, which showed 86 percent of the load in the boron fibers at the plane of discontinuity.

The stress distribution in the aluminum matrix for the transverse section model is shown in Figures 5.15 and 5.16. These plots represent the stress in the fiber axis direction (σ_z in this case) for the matrix material along the y-axis and along a line 45° to the y-axis. Both the stresses for an unflawed composite and one in which the fiber centered at x = y = 0 has an effective modulus of zero are shown. The applied stress is 2,000 psi. As these plots show, there is a definite change in stress levels when one fiber is deleted; the stress gradients between the fibers are quite low when compared to those seen in the longitudinal models. This of course is due to the fact that the transverse model can

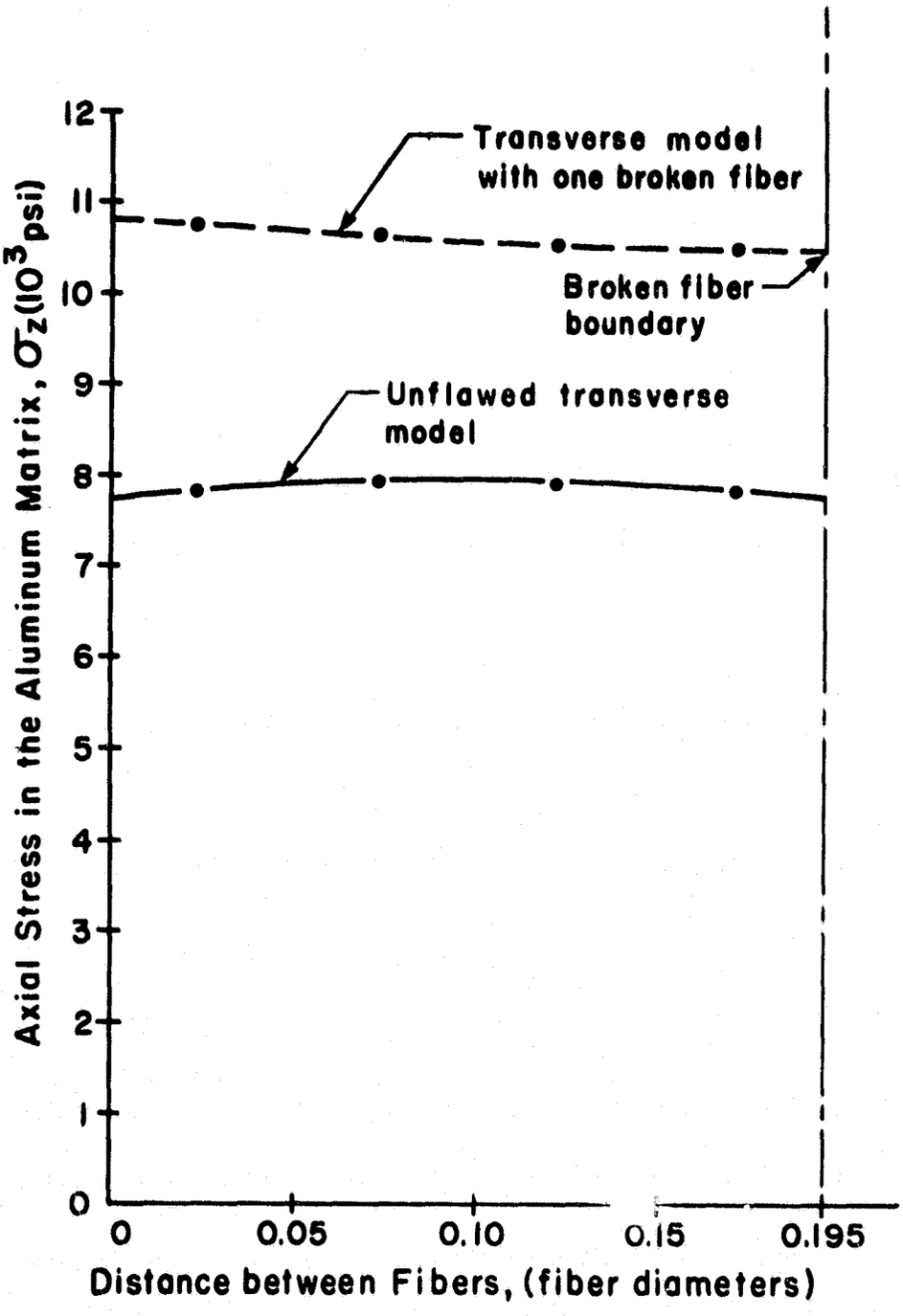

FIGURE 5.15

Axial Stress Distributions in the Aluminum Matrix, Transverse Model, 90° Section (minimum distance between fibers), Applied Stress $\bar{\sigma}_z$ = 29,000 psi

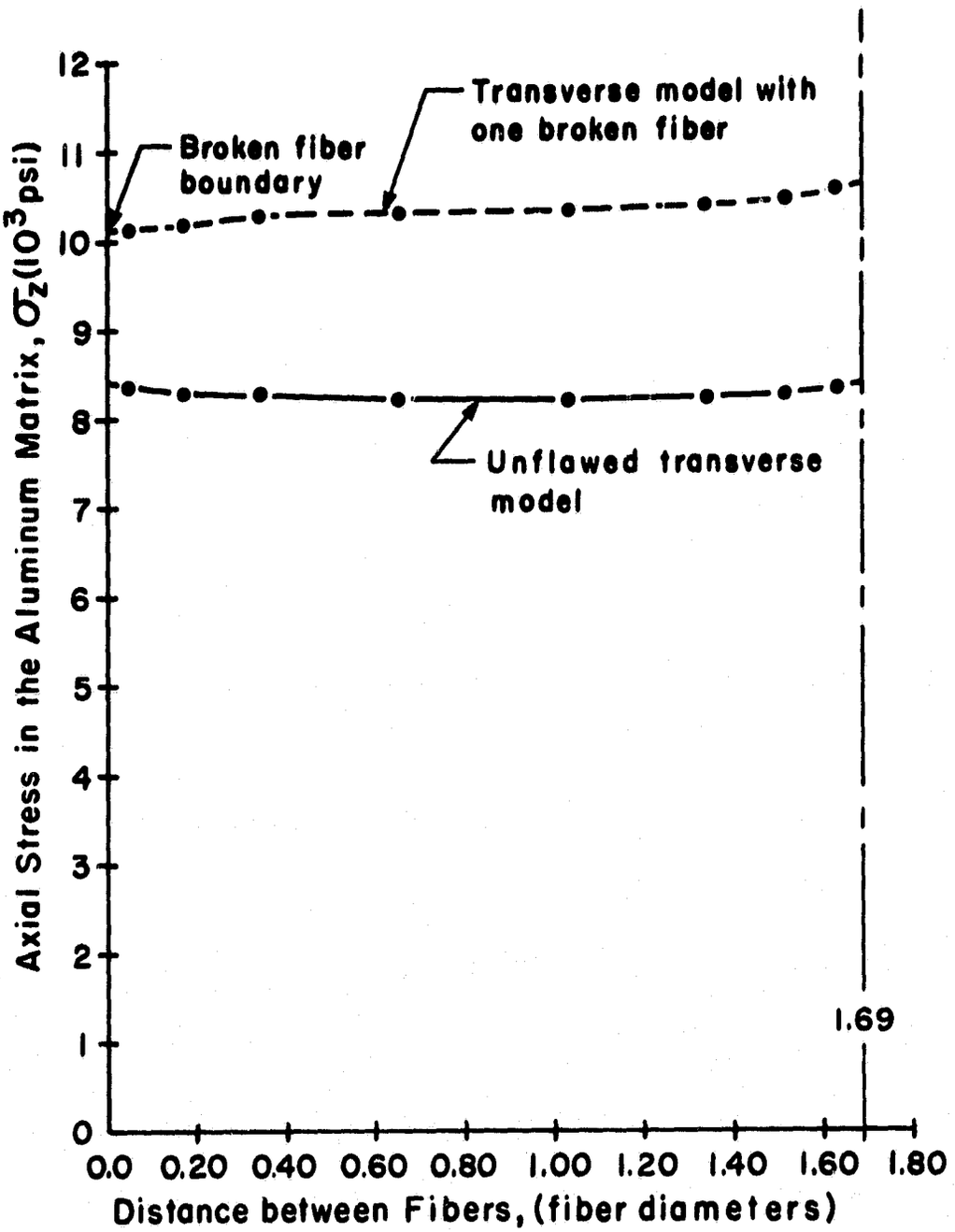

FIGURE 5.16

Axial Stress Distributions in the Aluminum Matrix, Transverse Model, 45° Section (maximum distance between fibers), Applied Stress $\bar{\sigma}_z$ = 29,000 psi

only represent differences in material properties caused by broken or reduced capacity fiber elements, but cannot account for the physical discontinuity of a fiber and the resulting stress concentrations. In fact, for both the unflawed case and the model in which one boron fiber is deleted, the variation in stresses in the axial or z-direction is no more than about 10 percent throughout the aluminum matrix, and considerably less then this in the boron elements.

The in-plane stresses, i.e., σ_x, σ_y, and τ_{xy}, show considerable variation in the aluminum matrix, but are about 10 orders of magnitude less than the axial stress. Contour plots for constant values of in-plane shear stress, and maximum and minimum principal stresses, are shown in Figures 5.17, 5.18, 5.19, 5.20, 5.21 and 5.22, for both the unflawed and flawed longitudinal models, to show the influence of deleting one fiber.

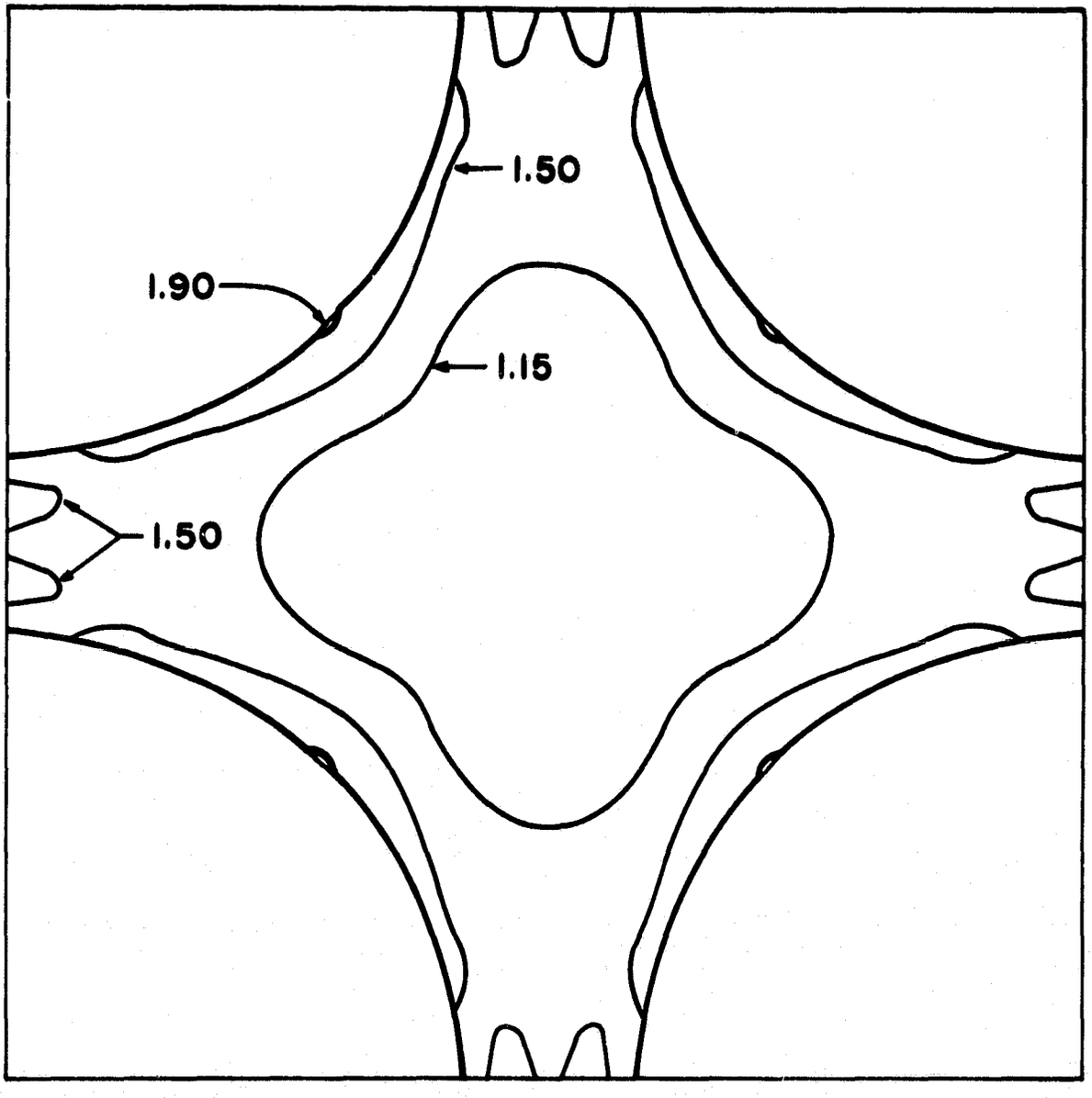

FIGURE 5.17

Maximum Principal Stress Contours (ksi), Unflawed Transverse Section Model, Applied Stress $\bar{\sigma}_z$ = 32 ksi

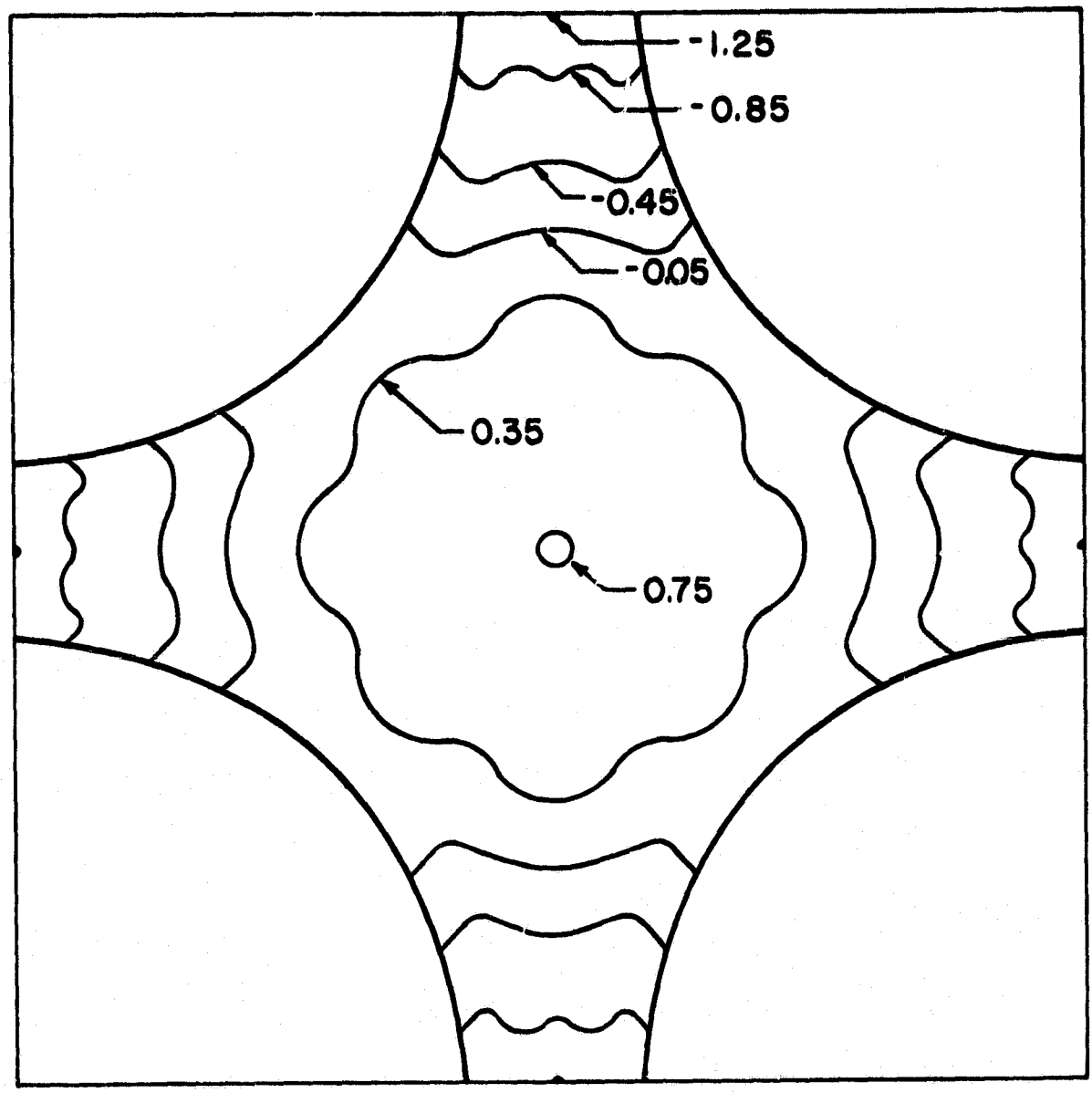

FIGURE 5.18

Minimum Principal Stress Contours (ksi), Unflawed Transverse Section Model, Applied Stress $\bar{\sigma}_z$ = 32 ksi

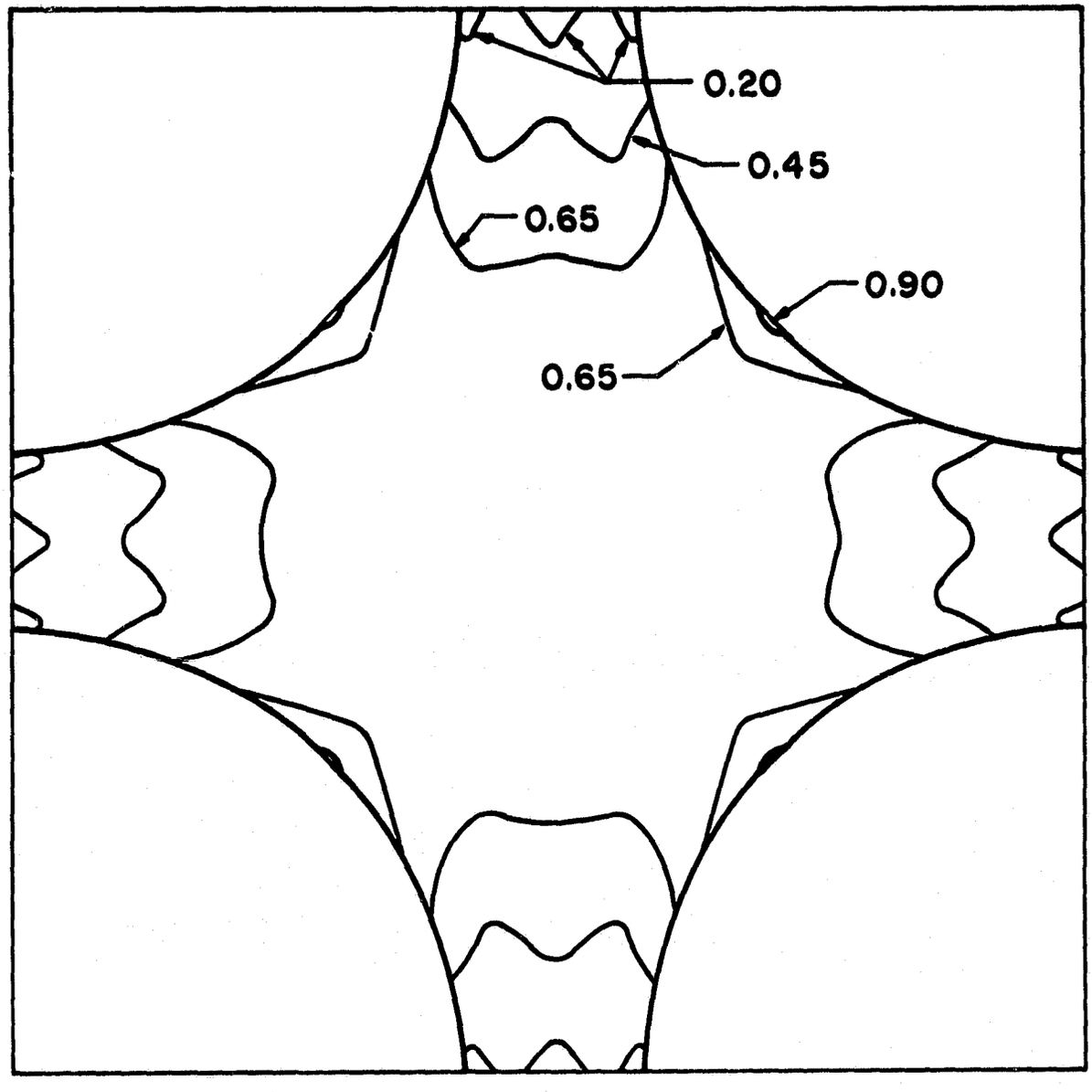

FIGURE 5.19

Shear Stress Contours (ksi), Unflawed Transverse Section Model, Applied Stress $\bar{\sigma}_z$ = 32 ksi

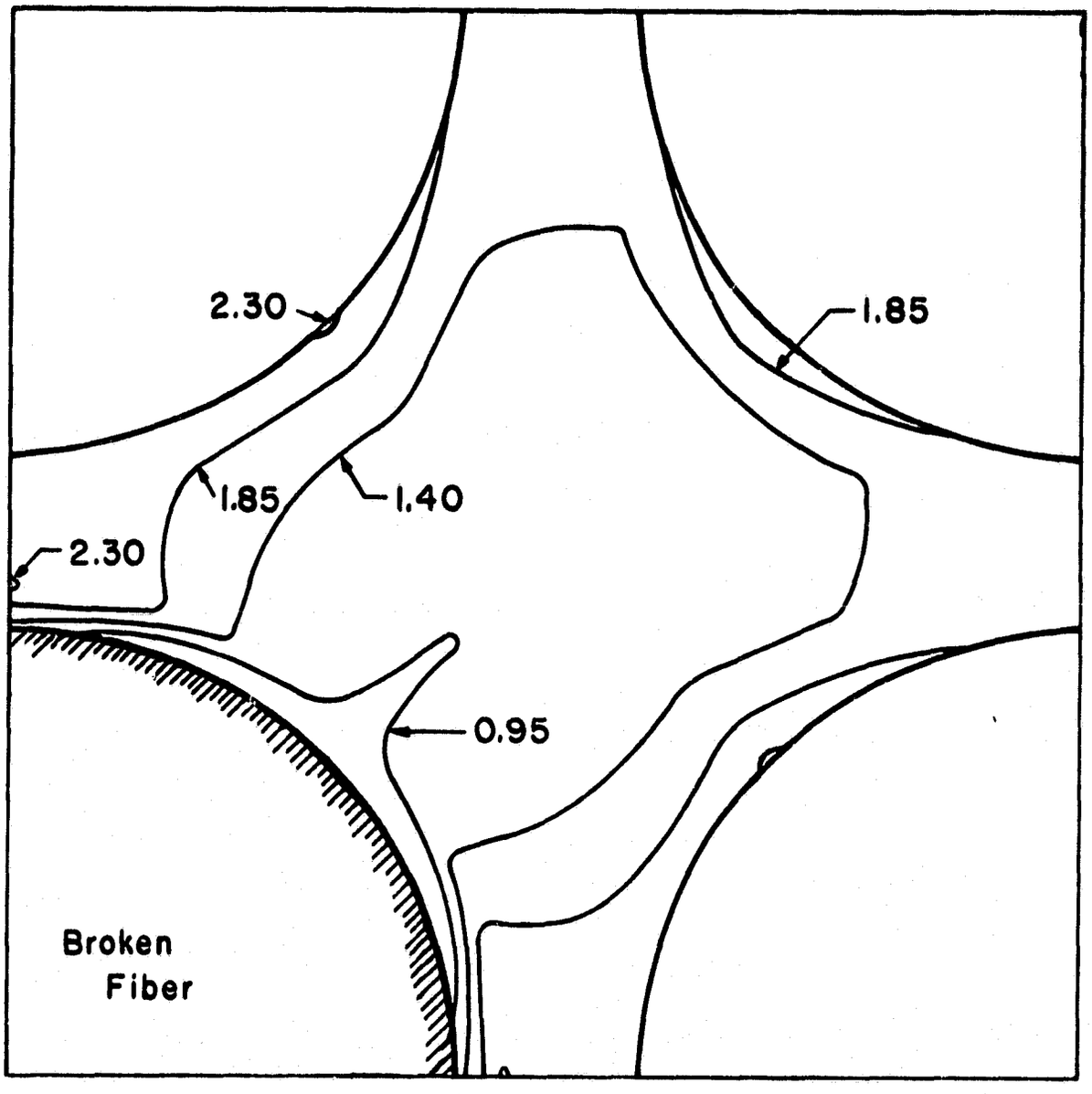

FIGURE 5.20

Maximum Principal Stress Contours (ksi), Transverse Section Model with One Broken Fiber, Applied Stress $\bar{\sigma}_z$ = 32 ksi

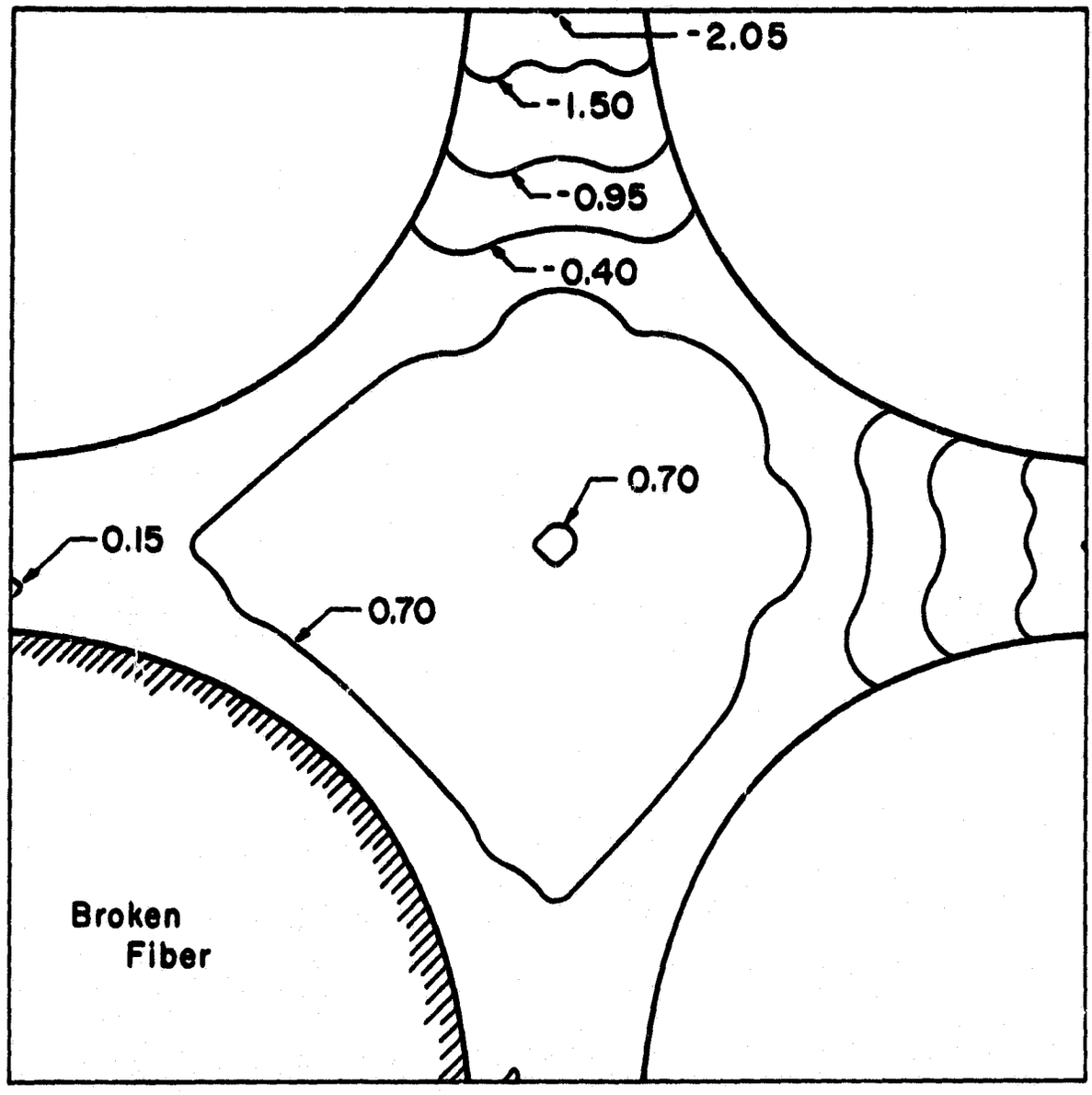

FIGURE 5.21

Minimum Principal Stress Contours (ksi), Transverse Section Model With One Broken Fiber, Applied Stress $\bar{\sigma}_z$ = 32 ksi

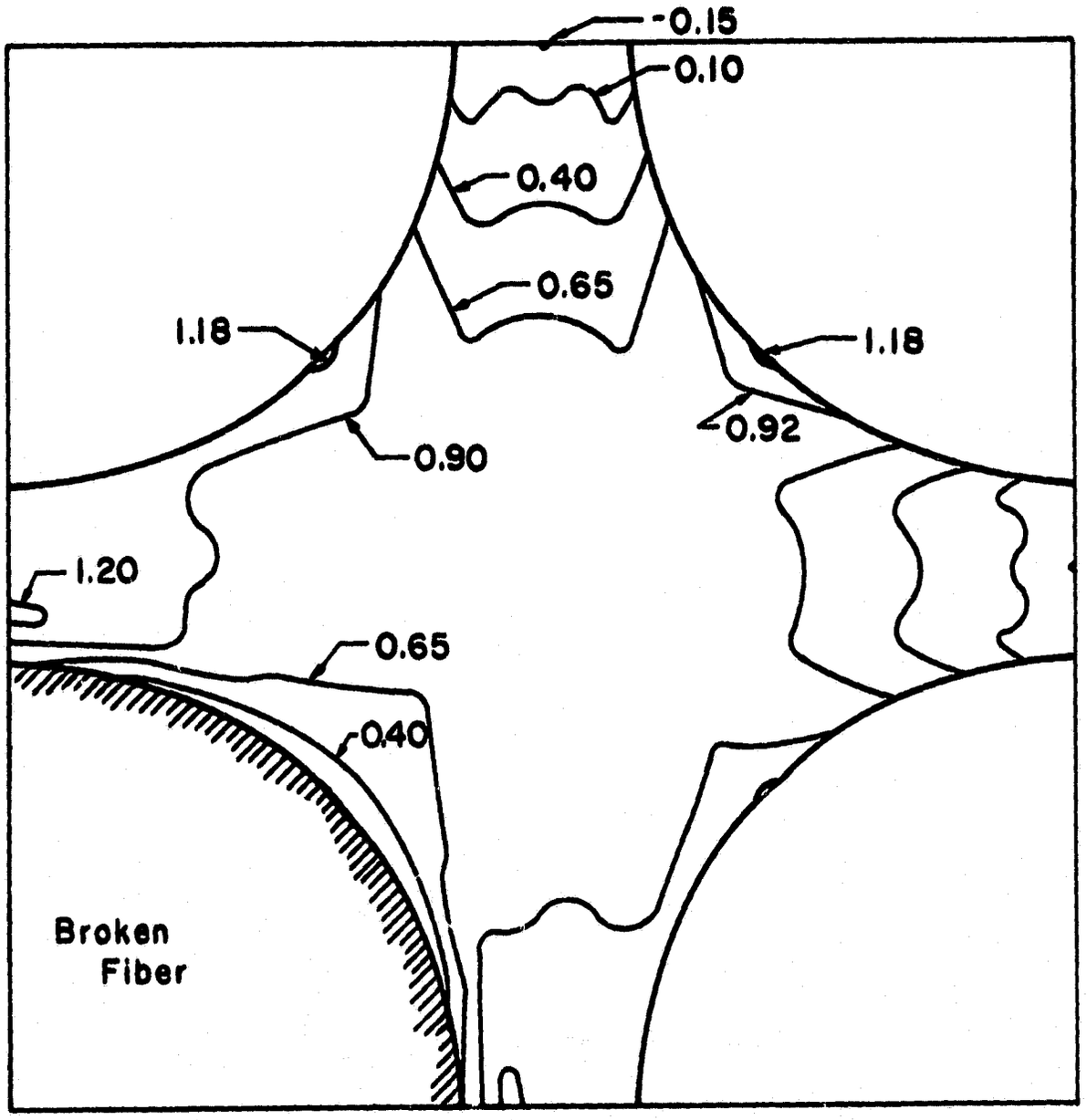

FIGURE 5.22

Shear Stress Contours (ksi), Transverse Section Model With One Broken Fiber, Applied Stress $\bar{\sigma}_z$ = 32 ksi

SECTION 6

FUTURE WORK

Debugging of the updated and corrected crack propagation version of the micromechanics computer program is nearly complete. Production runs using this program will soon be performed on the 45° and the 90° section models. Behavior in terms of crack propagation and energy absorption will be determined, and attempts to correlate these results to the experimental results of other investigators will be made. From experience to date with crack propagation analysis schemes, a further refinement of the 90° section longitudinal model appears desirable. Specifically, the aspect ratios of some of the finite elements are presently rather large; the region of uniform and small elements required to more accurately study crack growth will be extended. Once the energy absorption characteristics of these longitudinal models have been determined, several additional areas of interest will be explored.

Transverse loading of both longitudinal and transverse section models containing flaws will be of interest, particularly if these loading conditions are preceded by temperature gradients and hydrostatic loading increments to simulate the fabrication process for boron/aluminum. This "preconditioning" provides a prediction of the residual stresses and strains in the composite prior to mechanical loading, and could have a significant effect on the overall influence of internal flaws.

Finally, it has not been possible, to this point, to relate the stress concentration effects seen in a longitudinal model to a transverse section model. This would not be a serious problem were it not for the

differences in behavior observed in axial loading of the 90° and the 45° section models. Furthermore, in examining a transverse section of a typical square array unidirectional composite, as illustrated in Section 3.3, one can see that the fibers in closest proximity to a broken fiber, e.g., those represented by a 90° section model, will be affected in turn by their closest unflawed neighbors, some of which are the continuous fibers represented in a 45° section model. In effect, all of the fibers surrounding a broken fiber are coupled in the mechanism of load redistribution, and crack propagation is likely to be too complex to be characterized by a two-dimensional formulation. Until more extensive experimental data are available to verify and improve the present two-dimensional formulation, a three-dimensional finite element micromechanics analysis appears to be the logical approach to further understanding of energy absorption in metal-matrix composites. Such a program is in the final stages of development at the University of Wyoming, and during the second-year study, preliminary investigations of its applicability to the present problem will be made.

REFERENCES

1. Miller, A. K., and Adams, D. F., "Micromechanical Aspects of the Environmental Behavior of Composite Materials," Department Report UWME-DR-7011111, University of Wyoming, 1977.

2. Adams, D. F., "High-Performance Composite Materials for Vehicle Construction: An Elastoplastic Analysis of Crack Propogation in a Unidirectional Composite," Report R-1070-PR, The Rand Corporation, Santa Monica, California, March 1973.

3. Repnau, T., and Adams, D. F., "High-Performance Composite Materials for Vehicle Construction: A Finite Element Computer Program for the Elastoplastic Analysis of Crack Propagation in a Unidirectional Composite," Report R-1392-PR, The Rand Corporation, Santa Monica, California, October 1973.

4. Ko, W. L., "Finite Element Microscopic Stress Analysis of Cracked Composite Systems," Journal of Composite Materials, Vol. 12, January 1978, pp. 97-115.

5. Akbarzadeh, A., "Effect of Broken Fiber on the Strength of Unidirectional Composite Materials," Fibre Science and Technology, Vol. 11, No. 3, May 1978.

6. Awerbuch, J., and Hahn, H. T., "Crack Tip Damage and Fracture Toughness of Boron/Aluminum Composites," Journal of Composite Materials, Vol. 13, April 1979, pp. 82-107.

7. Adams, D. F., and Doner, D. R., "Transverse Normal Loading of a Unidirectional Composite," Journal of Composite Materials, Vol. 1, 1967, pp. 152-164.

8. Baker, J. D., and Foye, R. L., "Advanced Design Concepts for Advanced Composite Airframes," North American Rockwell Corporation, Technical Management Report No. 2 to the Air Force Materials Laboratory under Contract F33616-68-C-1199, October 1969.

9. Foye, R. L., "Inelastic Micromechanics of Curing Stresses in Composites," Inelastic Behavior of Composite Materials, Edited by C. T. Herakovich, The American Society of Mechanical Engineers, New York, 1975, pp. 172-211.

10. Crossman, F. W., "Computer Simulation of the Deformation of Composite Materials by Finite Element Analysis," Ph.D. Thesis, Department of Materials Science, Stanford University, Stanford, California, May 1972.

11. Karlak, R. R., and Crossman, F. W., "Failure Mechanisms in Composite Systems," Lockheed Palo Alto Research Laboratory, Palo Alto, California, Final Report to the U.S. Naval Air Systems Command under Contract N00019-74-C-0339, August 1975.

12. Dvorak, G. J., Rao, M. S. M., and Tarn, J. O., "Yielding in Unidirectional Composites Under External Loads and Temperature Changes," Journal of Composite Materials, Vol. 7, April 1973, pp. 194-216.

13. Adams, D. F., "Elastoplastic Crack Propagation in a Transversely Loaded Unidirectional Composite," Journal of Composite Materials, Vol. 8, January 1974, pp. 38-54.

14. Adams, D. F., and Miller, A.K., "Hygrothermal Microstresses in a Unidirectional Composite Exhibiting Inelastic Material Behavior," Journal of Composite Materials, Vol. 11, July 1977, pp. 285-299.

15. Lin, T. H., Salinas, D., and Ito, Y. M., "Initial Yield Surface of a Unidirectionally Reinforced Composite," Journal of Applied Mechanics, Series E, Vol. 39, No. 2, June 1972, pp. 321-326.

16. Lin, T. H., Salinas, D., and Ito, Y. M., "Elastic-Plastic Analysis of Unidirectional Composites," Journal of Composite Materials, Vol. 6, January 1972, pp. 48-60.

17. Ebert, L. J., Greisbach, T. J., and Flynn, P. L., "Finite Element Analysis System for the Mechanical Behavior of Oriented Fiber Composite Materials Under Combined Stresses," Technical Report AFOSR-TR-0042, Case Western Reserve University, Cleveland, Ohio, Sponsored by the Air Force Office of Scientific Research under Grant Number AFOSR-72-2374, June 1974.

18. Adams, D. F., "Inelastic Analysis of a Unidirectional Composite Subjected to Transverse Normal Loading," Journal of Composite Materials, Vol. 4, July 1970, pp. 310-328.

19. Heubner, K. H., The Finite Element Method for Engineers, Wiley-Interscience, New York, 1975.

20. Zienkiewicz, O. E., The Finite Element Method in Engineering Science, 3rd Edition, McGraw Hill, London, 1977.

21. Cook, R. D., Concepts and Applications of Finite Element Analysis, John Wiley and Sons, Inc., New York, 1974.

22. Murphy, D. P., and Adams, D. F., "Energy Absorption Mechanisms During Crack Propagation in Metal Matrix Composites," Quarterly Progress Report No. 1, performed under NASA-Lewis Grant NSG-3217, December, 1978.

23. Murphy, D. P., and Adams, D. F., "Energy Absorption Mechanisms During Crack Propagation in Metal Matrix Composites," Quarterly Progress Report No. 3, performed under NASA-Lewis Grant NSG-3217, June 1979.

24. Military Handbook 5A, "Metallic Materials and Elements for Aerospace Vehicle Structures," Department of Defense, Washington, D.C., 1966.

25. DiCarlo, J. A., "Mechanical and Physical Properties of Modern Boron Fibers," NASA Technical Memorandum NASA TM-73882, April 1978.

26. Lekhnitskii, S. G., Theory of Elasticity of an Anisotropic Elastic Body, Holden - Day, Inc., San Francisco, 1963.

27. Halpin, J. C., and Pagano, N. J., "Consequences of Environmentally Induced Dilatation in Solids, "Report AFML-TR-68-395, Air Force Materials Laboratory, Dayton, Ohio, December, 1969.

28. Whitney, J. M., and Ashton, J. E., "Effect of Environment on the Elastic Response of Layered Composite Plates," AIAA Journal, Vol. 9, No. 9, September 1971, pp. 1708-1713.

29. Bloom, J. M., and Adams, D. F., "Axial Loading of a Unidirectional Composite - Anisotropic Filaments," Journal of Composite Materials, Vol. 3, January 1969, pp. 186-188.

30. Branca, T. R., "Creep of a Unidirectional Metal Matrix Composite Subjected to Axial and Normal Lateral Loads," TAM Report 341, Department of Theoretical and Applied Mechanics, University of Illinois, Urbana, Illinois, sponsored by the U.S. Naval Air Systems Command under Contract N00019-71-C-323, June 1971.

31. Hill, R., The Mathematical Theory of Plasticity, Oxford University Press, London, 1950.

32. Richard, R. M., and Blacklock, J. R., "Finite Element Analysis of Inelastic Structures," AIAA Journal, Vol. 7, No. 3, March 1969, pp. 432-438.

APPENDIX A

FINITE ELEMENT FORMULATION OF THE MICROMECHANICS ANALYSIS COMPUTER PROGRAM

A.1 COORDINATES AND BOUNDARY CONDITIONS

To aid in the discussion of topics to follow, Figure A.1 is presented as representative of a typical repeating unit of a composite material under analysis, and Figure 3.2 defines some of the geometrical parameters describing a typical triangular element.

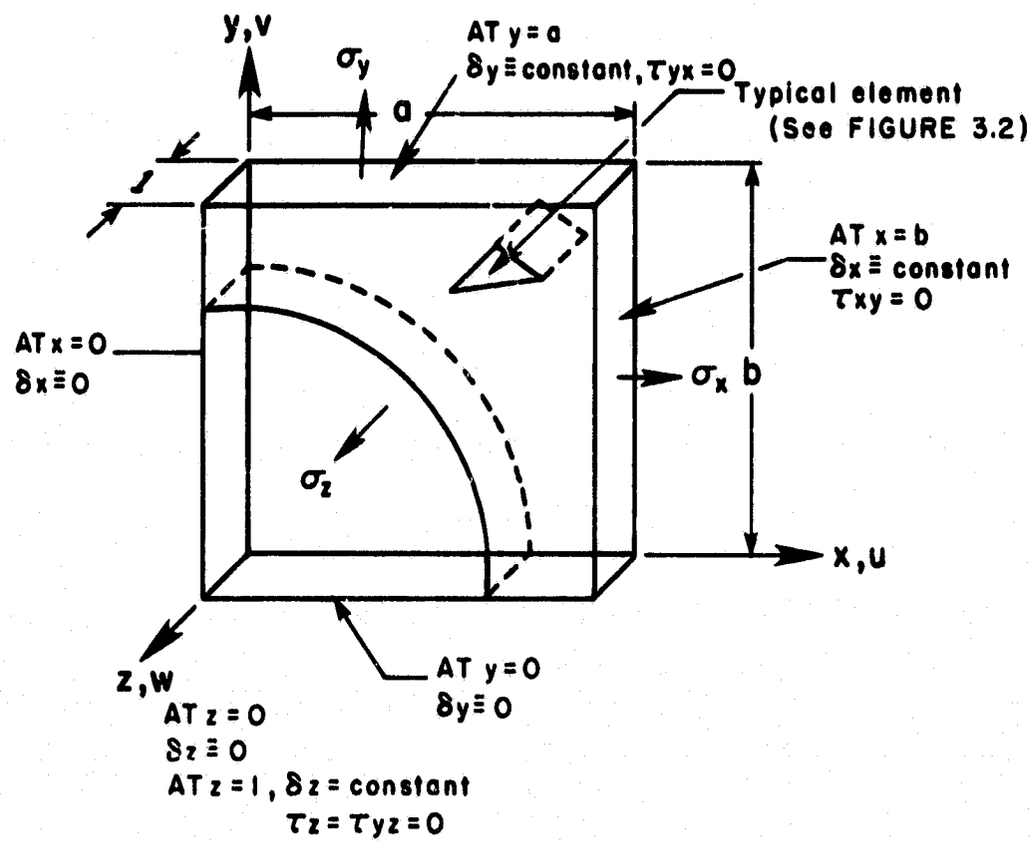

FIGURE A.1

Configuration of the Area of Interest for a Typical Micromechanics Analysis, Including Boundary Conditions

As discussed by Miller (pp. 32-42 of Reference [1]), the fiber packing geometry is assumed to be symmetric, and the repeating first quadrant unit of the composite continuum represented by Figure A-1 must remain rectangular when any combination of normal tractions, $\bar{\sigma}_x$, $\bar{\sigma}_y$, and $\bar{\sigma}_z$ are applied to the three orthogonal planes. This results in the specification of unique boundary conditions to maintain the symmetry and continuity of the material under investigation. These boundary conditions are explained in detail by Miller and Adams [1], and by Adams [2], and summarized in Figure A.1.

A.2 GENERALIZED PLANE STRAIN

In Miller's [1] formulation of the governing constitutive equations for the finite elements used in this analysis, generalized plane strain conditions were assumed in order to reduce the analysis to a quasi-three-dimensional problem. In past micromechanics investigations, finite element models representing a transverse section of a unidirectional composite were treated as ordinary plane strain problems. Under these conditions, the body under consideration is assumed to be thick, i.e., the axial dimension is much larger than the transverse dimensions, and the displacement in that direction is assumed to be zero, resulting in zero strain in that direction, i.e.,

$$\varepsilon_z = \gamma_{xz} = \gamma_{yz} = 0 \qquad \text{(A-1)}$$

For isotropic materials, this condition permits an induced normal stress in the axial direction of

$$\sigma_z = \nu(\sigma_x + \sigma_y) \qquad \text{(A-2)}$$

Miller's primary reason for incorporating generalized plane strain conditions was to allow axial loading, i.e., loading parallel to the fiber axes, the z-direction in his transverse section finite element grids (see

Figure A-1). In addition, when a composite is loaded in the transverse direction with no longitudinal tractions being applied, the generalized plane strain conditions allow a normal strain to develop along the longitudinal axis, resulting in zero stress in the longitudinal direction.

Lekhnitskii [26] defines generalized plane strain in a very general manner, stating that all of the strains associated with the z-axis direction can be nonzero constants, including the shear strains, γ_{xz} and γ_{yz}. In the current analysis, a somewhat less general form of generalized plane strain has been employed in which it is assumed that only the normal strain, ε_z is nonzero, i.e., γ_{xz} and γ_{yz} are assumed to be zero. This definition requires that all planes perpendicular to the z-axis direction be a linear function of the position coordinates in that direction, i.e.,

$$\omega = \kappa z \tag{A-3}$$

where κ is a constant. In other words, some constant strain, ε_z, exists in the z-axis direction

$$\varepsilon_z = \frac{\partial \omega}{\partial z} = \kappa \tag{A-4}$$

This means that the displacements of all of the node points in the z-axis direction are identical. It is also important to note that the axial stress, σ_z, is uncoupled from the transverse stresses, σ_x, σ_y, and τ_{xy}. Keeping this in mind and referring to Figure 3.2, the following points are noteworthy:

a) Node points i', j', and k' are required to have the same displacements in the x and y directions as points i, j, and k.

b) Node points i, j, and k have identical displacements in the z-directions, while from symmetry considerations, i', j', and k' have zero displacements in the z-direction.

c) Since each element is assumed to be of unit thickness, the displacements of the unprimed node points in that direction represent

the strain, ε_z.

A.3 FORMULATION OF ELEMENTAL STIFFNESS MATRICES BASED ON GENERALIZED PLANE STRAIN CONDITIONS

The full development of the basic finite element method is available in complete detail in several texts (References [19-21], for example), and a complete examination of the formulation and assembly process resulting in a set of simultaneous algebraic equations will therefore not be included here. Only a brief overview of the process is presented so that the unique capabilities of the present analysis scheme might be better explained.

Once the assumed displacement field within each element has been expressed in terms of unknown node point displacements (see Figure 2.1), the strain at any point within the element can be expressed as

$$\varepsilon_{ij} = \tfrac{1}{2}\left(\frac{\partial u_i}{\partial x_j} + \frac{\partial u_j}{\partial x_i}\right) \qquad \text{(A-5)}$$

with $i = 1,2$
$u_1 = u$ = x-displacement
$u_2 = v$ = y-displacement
$x_1 = x$
$x_2 = y$

As a result, a general expression relating the strains to the displacements in any element, i, can be written as

$$\{\varepsilon\}_i = [B]_i \{\delta\}_i \qquad \text{(A-6)}$$

The matrix $[B]_i$ is a set of geometric parameters relating the vector of the node point displacements, $\{\delta\}_i$, to the strains in the i-th element. The form of $[B]_i$, generally known as the "shape" matrix, is dependent on the form of the assumed displacement field.

The stresses and strains are related by an appropriate constitutive relationship, Hooke's law being a familiar example. The general Duhamel-

Neumann form of these constitutive relationships [20, 27, 28] is

$$\{\sigma\} = [H]\,(\{\varepsilon\} - \{\varepsilon_o\}) \tag{A-7}$$

Where $\{\sigma\}$ and $\{\varepsilon\}$ are the stress and strain vectors, respectively, and $[H]$ is a matrix containing the appropriate material properties relating the two. The elements of the initial strain vector, $\{\varepsilon_o\}$, are dilatational strains induced by thermal or moisture changes. This topic will be discussed in greater detail in Section A.5.2 of this Appendix, but for now it is noted that the temperature and moisture sensitive matrix materials have an order of symmetry which is at least orthotropic, so that dilatational shear strains cannot exist. That is, the initial strain vector can be expressed as

$$\{\varepsilon_o\} = \begin{Bmatrix} \varepsilon_{x_o} \\ \varepsilon_{y_o} \\ \varepsilon_{z_o} \end{Bmatrix} \tag{A-8}$$

As described by Zienkiewicz [20] for instance, an expression for the strain energy within an element can be written using the relationships given above, leading to an expression for a potential energy functional in terms of strain energy and forces acting at the node points. Minimization of this functional results in a set of simultaneous algebraic equations relating node point forces to node point displacements. Typically,

$$\{F\}_i = [k]_i\{\delta\}_i + \{F_{\varepsilon_o}\}_i \tag{A-9}$$

where $\{F\}_i$ is the vector of forces acting on the node points of element i, and $[k]$ is the stiffness matrix for element i. The elements of the vector $\{F_{\varepsilon_o}\}_i$ are the forces acting on the node points resulting from initial dilatational strains developed within the element. For constant strain elements, the form of $[k]_i$ is

$$[k]_i = [B]_i^T [H]_i [B]_i t_i \Delta_i \qquad \text{(A-10)}$$

where t_i is the thickness of the element and Δ_i is the area of element i in the x-y plane.

All of the forces on each node point in an array due to each element sharing that node point must be in equilibrium. In addition, the summation of all such node point forces must be in equilibrium with all externally applied loads and specified boundary restraints. This equilibrium requirement and the summation process it entails leads to the formation of a "global" stiffness matrix, [K], for the entire region under analysis. What this essentially does is to assemble all of the equations of the form of (A-9) for all elements, resulting in a total set of simultaneous equations for the entire area being analyzed.

$$\{F\} = [K]\{\delta\} + \{F_{\varepsilon_o}\} \qquad \text{(A-11)}$$

For our constant strain element, the displacement fields under generalized plane strain conditions are

$$\begin{aligned} u &= a_1 + a_2 x + a_3 y \\ v &= b_1 + b_2 x + b_3 y \\ w &= \kappa z \end{aligned} \qquad \text{(A-12)}$$

where κ is a constant.

For the triangular element shown in Figure 3.2, the coefficients A_1, A_2, A_3, b_1, b_2, and b_3 can all be expressed in terms of the node point displacements in the x-y plane. This leads to the shape matrix $[B]_i$ as developed by Heubner [19], but with a fourth row and a seventh column added to express the condition of generalized plane strain:

where $\varepsilon_o' = \alpha'\Delta T + \beta'\Delta M$

For a complete discussion of the derivation of the material properties matrices shown above, the interested reader will find a thorough and easily understood development by Miller and Adams (pp. 47-53 and Appendices A and C of Reference [1]). It is to be noted that while these expressions for $[H]_1$ involve the region of elastic or linear stress-strain behavior, the values of the material constants E, ν, α, β, etc., can be functions of temperature and moisture.

A4.0 LOAD APPLICATION

Loads introduced to the finite element array in the micromechanics analysis can be in the form of applied mechanical tractions, or arise from thermally or moisture induced dilatations. Mechanical loading can consist of average applied normal stresses in the x, y, and z directions, as defined by Figure A-1, for each load increment, while thermal and moisture gradients can be applied at any increment to reflect environmental changes the composite may be subjected to. Mechanical loading will be discussed first.

The application of mechanical tractions to the finite element model is considerably simplified by taking advantage of the boundary conditions, as specified in Figure A-1, which permits a rearrangement of the global stiffness matrix [K], and the total force vector, {F}, by a method introduced by Branca [30]. The displacement boundary conditions for the repeating unit finite element model were specified in order to maintain continuity of the material continuum under investigation. Specifically, referring again to Figure 2.1, displacements in the x-direction of node points along the right-hand vertical boundary must be uniform. Displace-

PRECEDING PAGE BLANK NOT FILMED 75-76

ments in the y-direction of the upper horizontal boundary must be uniform, and the displacements of all node points in the z-axis direction must be uniform. When the overall force-displacement equation of the system is considered, i.e.,

$$\{F\} = [K]\{\delta\} \tag{A-18}$$

one can see that all of the boundary node points involved in mechanical loading will have identical displacements with respect to the direction of the load application. These identical displacements allow combining of certain terms in the global stiffness matrix that result in the replacement of the applied forces on boundary nodes by zeroes, in the manner described by Branca [30]. Successive modification of the global stiffness matrix for each boundary node point displacement results in the following form of Equation (A-18) for the simultaneous application of uniform values of σ_x, σ_y, and σ_z for an array of n nodal points

$$\begin{Bmatrix} 0 \\ 0 \\ 0 \\ \cdot \\ \cdot \\ \cdot \\ \bar{F}_x \\ \bar{F}_1 \\ \bar{F}_z \end{Bmatrix} = \begin{bmatrix} k_{11} & k_{12} & k_{13} & \cdots & k_{1(2n+2)} \\ & k_{22} & k_{23} & \cdots & \\ & & k_{33} & & \\ & & & - & \\ & & & & - \\ & & & & \\ & & & & \\ & & & & \\ \text{symmetric} & & & & - \end{bmatrix} \begin{Bmatrix} \delta_1 \\ \delta_2 \\ \delta_3 \\ \cdot \\ \cdot \\ \cdot \\ \delta_{2n} \\ \delta_{2n+1} \\ \delta_{2n+2} \end{Bmatrix} \tag{A-19}$$

where $\bar{F}_x$, $\bar{F}_y$, and $\bar{F}_z$ are the total applied loads in the x, y, and z directions, and are defined, for a unit thickness model, as

$$\begin{aligned} \bar{F}_x &= \sigma_x b \\ \bar{F}_y &= \sigma_y a \\ \bar{F}_z &= \sigma_z ab \end{aligned} \tag{A-20}$$

where a and b are as defined in Figure 2.1. On pp. 63-67 of Reference [1], Miller clearly illustrates, by means of a simple two-element model, the manner in which the elements of the global stiffness matrix are manipulated to obtain Equation (A-19). The important point is that this procedure allows a rather straightforward simultaneous application of external tractions in the directions of the three coordinate axes.

Thermal-dilatational and moisture-dilatational effects are also included within a given loading increment. These effects appear as the vector $\{F_{\varepsilon_o}\}_i$ in Equation (A-9). The elements of this vector represent the forces on the node points of an element which are the result of dilatational strains, ε_o, due to thermal and moisture gradients, as given by Equation (A-15). The magnitudes of these induced nodal forces are a function of the shape of the element, [B], and its material properties, [H], i.e.,

$$\{F_{\varepsilon_o}\}_i = -[B]_i^T[H]_i\{\varepsilon_o\}_i t_i A_i \qquad \text{(A-21)}$$

When a loading increment includes a change in temperature or moisture content, the node point forces given by Equation (A-21) are calculated and then moved to the right-hand side of Equation (A-9)

$$\{F-F_{\varepsilon_o}\}_i = [k]_i\{\delta\}_i \qquad \text{(A-22)}$$

This form is retained when the elemental equations are assembled into the total global form, as given by Equation (A-11), so that a single loading vector exists for each increment and only one inversion of the total stiffness matrix, [K], is required.

A.5 NONLINEAR MATERIAL RESPONSE

The University of Wyoming micromechanics analysis program models the response of the isotropic matrix of composite materials to both external tractions and changes in temperature and/or moisture concentrations. Be-

cause the vast majority of matrix materials in use today are capable of considerable plastic deformation before failure, an elastoplastic analysis scheme for deformation due to mechanical loading is essential for micromechanics studies. In addition, the effects of temperature and moisture (hygrothermal) changes must be considered. Internal stresses induced by the high temperature fabrication and bonding processes that most composites are subject to can actually cause material failures before any mechanical load is applied, while the effects of moisture absorption by polymeric resins has become an area of major concern for analysts and designers in recent years. Past micromechanics studies [2, 3, 7-18] have assumed that the material properties remain constant for all states of temperature and moisture to which the constituent materials are exposed. This is not the case, as these changes in temperature and moisture content not only induce stresses, but at the same time significantly alter the material properties. This is also a type of nonlinear behavior and it must be accounted for. A brief description of the manner in which the effects of plasticity and the hygrothermal dependence of the material properties are incorporated into the finite element stiffness matrix follows in the next two subsections.

A.5.1 ISOTROPIC MATERIALS IN THE PLASTIC REGION UNDER GENERALIZED PLANE STRAIN CONDITIONS

Of the many elastoplastic finite element analyses of undirectional composites performed to date [2, 3, 8-11, 13, 16, 18], the present procedure is most like that described by Adams [13]. It is modified to account for the generalized plane strain assumptions and for the inclusion of the effects of environmental changes. Like most methods of approximating nonlinear material behavior, the present procedure requires that loading be

applied in small increments. This necessitates the accumulation of displacements, stresses and strains from each succeeding increment. It will be shown that this is possible due to the fact that the material properties used in incremental techniques are linear and therefore superposition principles apply.

Two basic techniques exist for accounting for the plastic portion of each loading increment: the tangent modulus method and the method of initial strains. The method of initital strains uses the elastic material properties, as employed in Equation (A-14), throughout the entire loading sequence. It accounts for plastic strain by adding an initial strain to the strain vector of each element and then iterating until equilibrium conditions are satisfied. The advantage of this method is that the global stiffness matrix [K] need only be formed and inverted once. The tangent modulus method uses the tangent modulus of the material at a particular stress-strain state to define the stiffness of each finite element for the next loading increment. While no iteration is required, a new global stiffness matrix must be assembled and inverted for every loading increment. A more detailed description of both of these methods is given by Adams (pp. 36-39 of Reference [2]), wherein the tangent modulus method emerges as being preferred for materials that exhibit relatively "flat" stress-plastic strain curves, which is the case for many metal matrix materials used in advanced composite materials. The current analysis uses the tangent modulus method for this reason. In addition, since the material properties must be modified at the beginning of each loading increment to account for environmental factors, which also requires the assembly of a new global stiffness matrix, use of the tangent modulus method imposes no penalty.

For each loading increment beyond the elastic limit, the corresponing increment of strain for any element can be separated into an elastic (recoverable) and a plastic (irrecoverable) part, or in Adams' notation [2],

$$\dot{\varepsilon}_{ij} = \dot{\varepsilon}_{ij}^{(e)} + \dot{\varepsilon}_{ij}^{(p)} \qquad \text{(A-23)}$$

where the elastic portion, $\dot{\varepsilon}_{ij}^{(e)}$, behaves according to the generalized Hooke's law,

$$\dot{\varepsilon}_{ij}^{(e)} = \frac{1-2\nu}{3E}\,\dot{\sigma}_{kk}\delta_{ij} + \frac{1+\nu}{E}\,\dot{s}_{ij} \qquad \text{(A-24)}$$

where δ_{ij} is the Kronecker delta, and $\dot{s}_{ij}$ is the deviatoric component of the rate of stress tensor,

$$\dot{s}_{ij} = \dot{\sigma}_{ij} - \frac{1}{3}\,\dot{\sigma}_{kk}\dot{\delta}_{ij} \qquad \text{(A-25)}$$

For this analysis, the plastic portion of the deformation is assumed to follow the Prandtl-Reuss flow rule [31],

$$\dot{\varepsilon}_{ij}^{(p)} = \dot{\lambda}s_{ij} \qquad \text{(A-26)}$$

where $\dot{\lambda}$ is a positive scalar function. In other words, at any instant, the rate of change of the plastic strain is proportional to the deviatoric stress only. The mean normal, or dilatational, strain makes no contribution to plastic deformation. Adams (pp. 13-15 of Reference [2]), goes through a detailed explanation of the procedure involved in obtaining a convenient form of $\dot{\lambda}$:

$$\dot{\lambda} = \frac{\dot{\tau}_o}{2\tau_o M_t} \qquad \text{(A-27)}$$

where τ_o is the octahedral shear stress

$$\tau_o = (1/3\; s_{ij}s_{ij})^{1/2} \qquad \text{(A-28)}$$

$\dot{\tau}_o$ is the octahedral shear stress rate of change, and $2M_t$ is the tangent modulus of the octahedral shear stress-octahedral plastic shear strain curve

$$2M_t = \frac{d\tau_o}{d\varepsilon_o^{(p)}} \qquad \text{(A-29)}$$

a linear relationship. The above equations lead to an incremental constitutive equation for elastoplastic material behavior

$$\dot{\varepsilon}_{ij} = \frac{1+\nu}{E}\dot{\sigma}_{ij} - \frac{\nu}{E}\dot{\sigma}_{kk}\delta_{ij} + \frac{s_{ij}s_{kl}\sigma_{kl}}{6\tau_o^2 M_T} \qquad \text{(A-30)}$$

Miller [1] adds an additional term to this expression to account for the dilatational strain increments induced by the environmental changes. Thus,

$$\dot{\varepsilon}_{ij} = \frac{1+\nu}{E}\dot{\sigma}_{ij} - \frac{\nu}{E}\dot{\sigma}_{kk}\delta_{ij} + \frac{s_{ij}s_{kl}\dot{\sigma}_{kl}}{6\tau_o^2 M_T} + \dot{\varepsilon}_o\delta_{ij} \qquad \text{(A-31)}$$

Equation (A-31) must be inverted in order to obtain the constitutive relationship in the form of Equation (A-6). Details of this inversion procedure under generalized plane strain conditions are given by Miller (Appendix D of Reference [1]). The resulting material properties matrix, [H], is

$$[H] = \frac{E}{1+\nu}\begin{bmatrix} \left(\frac{1-\nu}{1-2\nu} - \frac{s_{11}^2}{B}\right) & \left(\frac{\nu}{1-2\nu} - \frac{s_{11}s_{22}}{B}\right) & \left(-\frac{s_{11}s_{12}}{B}\right) & \left(\frac{\nu}{1-2\nu} - \frac{s_{11}s_{33}}{B}\right) \\ & \left(\frac{1-\nu}{1-2\nu} - \frac{s_{22}^2}{B}\right) & \left(-\frac{s_{22}s_{12}}{B}\right) & \left(\frac{\nu}{1-2\nu} - \frac{s_{22}s_{33}}{B}\right) \\ & & \left(\frac{1}{2} - \frac{s_{12}^2}{B}\right) & \left(-\frac{s_{12}s_{33}}{B}\right) \\ \text{symmetric} & & & \left(\frac{1-\nu}{1-2\nu} - \frac{s_{33}^2}{B}\right) \end{bmatrix} \qquad \text{(A-32)}$$

where $B = 3\tau_o^2\left[1 + (1+\nu)\frac{2M_t}{E}\right]$

and the elements of the incremental dilatational strain vector are

$$\{\dot{\varepsilon}_o\} = \begin{Bmatrix} \dot{\varepsilon}_o \\ \dot{\varepsilon}_o \\ 0 \\ \dot{\varepsilon}_o \end{Bmatrix} \qquad \text{(A-33)}$$

where $\dot{\varepsilon}_o = \alpha\Delta\dot{T} + \beta\Delta\dot{M}$ (A-34)

$\dot{\Delta T}$ and $\dot{\Delta M}$ representing the incremental changes in temperature and moisture content, respectively. Thus, for each matrix material element that has exceeded its elastic limit at a particular temperature and moisture condition, Equation (A-32) is used to define its material properties so that its elemental stiffness matrix, Equation (A-9), can be formed and incorporated into the global stiffness matrix, [K], for the current load increment.

An additional feature of the present analysis is that it is not restricted to monotonic loading. That is, unloading from the plastic region is possible for those elements that undergo stress relief due to local deformation or crack formation. It is assumed that the material unloads linearly elastically, with a modulus equal to the elastic modulus. If total unloading were to occur, the total plastic strain sustained by the element up to the point of unloading would be retained. If reloading subsequently occurs, the material follows the stress-strain response described by the elastic modulus until it attains the stress level from which it began to unload. For any loading past this point, the material continues to move along the original elastoplastic curve.

A.5.2 HYGROTHERMAL DEPENDENCE OF MATERIAL PROPERTIES

As noted previously, the alteration of the properties of the constituent materials of a composite as they are exposed to a changing environment has a significant effect on the microstress state of the composite. The present analysis scheme evaluates the stress-strain behavior, the coefficient of thermal expansion, the coefficient of moisture dilatation, the yield strength, the ultimate strength, and the ultimate strain for each element at the beginning of each load increment.

Many past elastoplastic analyses have input the entire stress-strain

response of the material under study as data tables, utilizing considerable amounts of core storage or peripheral storage in the process. If one were to do this for each stress-strain curve corresponding to a range of temperatures and moisture levels, a prohibitive amount of storage would be required, and even on today's larger computers, this would significantly limit the size of model that could be analyzed. The present analysis uses a three-parameter model to parametrically describe the stress-strain curve of a material at any temperature and moisture of interest. The model used is based on the Richard-Blacklock equation [32], which is capable of accurately modeling material behavior which exhibits large amounts of plastic deformation. The general form of the Richard-Blacklock equation is

$$\sigma = \frac{E\varepsilon}{\left(\left| \frac{E\varepsilon}{\sigma_o} \right|^n \right)^{1/n}} \qquad \text{(A-35)}$$

where E is the elastic modulus of the material and σ_o and n are independent parameters as illustrated in Figure A.2.

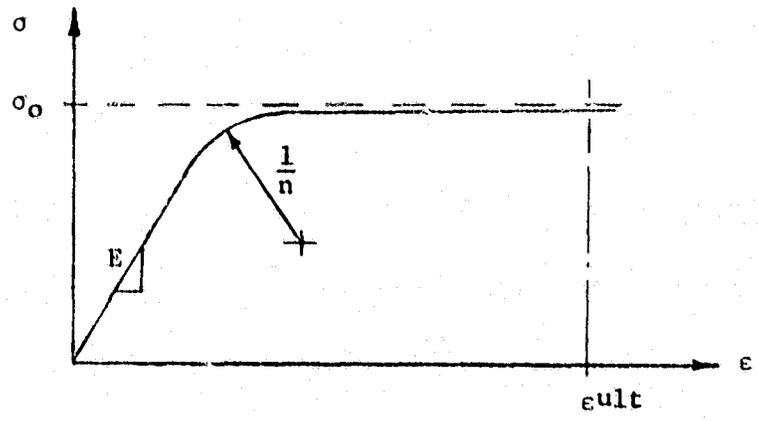

FIGURE A.2

Richard-Blacklock Representation of Stress-Strain Curves

For the present analysis, Equation (2.35) is modified to describe an octahedral shear stress-octahedral plastic shear strain curve, as the primary material failure criterion employed is the ultimate octahedral shear stress criterion. Fortunately, uniaxial test data for a given material can be converted directly to octahedral shear stress and strain. The octahedral form of Equation (A.35) is

$$\tau_o = \frac{\bar{E}\bar{\epsilon}}{\left[1+\left|\frac{\bar{E}\bar{\epsilon}}{\bar{\sigma}_o}\right|^n\right]^{1/n}} \qquad \text{(A-36)}$$

where τ_o is the octahedral shear stress as defined by Equation (A-28), and τ_o and n are again independent parameters which fit the curve to empirical data by means of a numerical least squares curve fit procedure (p. 76 of Reference [1]). The term $\bar{\epsilon}$ is the octahedral shear strain, defined as

$$\bar{\epsilon} = (1/3\ \epsilon_{ij}\epsilon_{ij})^{\frac{1}{2}} \qquad \text{(A-37)}$$

and $\bar{E}$ is the slope of the initial linear portion of the octahedral shear stress-octahedral shear strain curve, being related to the elastic modulus, E, as follows

$$\bar{E} = \left(\frac{2}{3(1+2\nu^2)}\right)^{\frac{1}{2}} \qquad \text{(A-38)}$$

The tangent modulus of the octahedral shear stress-plastic octahedral shear strain curve, $2M_T$, is the quantity required in forming the material properties matrix, [H], shown in Equation (A-32). The tangent modulus, $2M_T$, can be related to the tangent modulus, $\bar{E}_T$, of the octahedral shear stress-octahedral shear strain curve by

$$2M_T = \frac{\bar{E}\bar{E}_T}{\bar{E}-\bar{E}_T} \qquad \text{(A-39)}$$

where $\bar{E}_T$ can be obtained by differentiating Equation (A-36) with respect to $\bar{\varepsilon}$. This yields

$$\bar{E}_T = \frac{\bar{E}}{\left[1+\left|\frac{\bar{E}\bar{\varepsilon}}{\bar{\sigma}_o}\right|^n\right]^{1/n}} \qquad \text{(A-40)}$$

Thus, for a given octahedral shear strain, the tangent modulus, $2M_T$, can readily be calculated. It has been found that small changes of temperature or moisture do not drastically alter the stress-strain curve of a matrix material, but rather modify the material properties in a uniform manner. In other words, a functional relationship between the parameters σ_o, n and the elastic modulus, E, and temperature and moisture states can be found. This is done by fitting Equation (A-36), in a least squares sense, to octahedral shear stress-octahedral shear strain curves obtained from tensile test results in various environments. A somewhat more detailed description of this procedure is available on pp. 73-78 of Reference [1].